Composite and disaggregated maps as preliminary aids to analysis of manganese nodule geochemistry.

by

Joseph Moses Botbol [1]

U.S. Geological Survey Open File Report 92-559

October 14, 1992

[1]U.S. Geological Survey, Branch of Atlantic Marine Geology, Woods Hole, MA 02543

Table of contents

List of tables

List of figures

Abstract

Geochemical data from a data-base of globally distributed manganese nodule characteristics are mapped as grey-levels in both disaggregated and conventional composite form. Class number ranges are used instead of actual weight-percent in order to facilitate comparisons between variables. For multiple variable comparisons, the disaggregated maps, one for each concentration range in its companion composite map, reduce the likelihood of "next-step" investigation of apparently rich targets that are truly barren, and provide greater facility in correlating the variables with geological and geochemical features than conventional composite maps alone.

Introduction

Deep sea manganese nodules are recognized as a potential resource of nickel, copper, manganese and, to a lesser extent, cobalt. Few studies have been oriented toward detailed specification of the nature and distribution of nodule geochemistry on a global basis (McKelvey, 1983; Lenoble, 1992).

Overview of manganese nodules

The economic potential of marine manganese nodules has been a serious consideration for many years. As yet, no commercial extraction and beneficiation has taken place, but presently there is serious activity regarding development of nodules as a viable metal resource (Lenoble, 1992).

The nature of the nodules and their distribution has been studied to the extent that spatial distributions of many of their geochemical attributes are publicly available in data bases. This report deals with a global distribution of manganese nodule geochemical data that are widely spaced and were not captured with spatial continuity as a major controlling factor of their sample design.

Purpose

The purpose of this report is to demonstrate the nature and potential utility of the spatial distributions of disaggregated attributes of marine manganese nodule geochemical data. Moreover, the author wishes to demonstrate the pre-multivariate analysis benefits that can be derived from simple yet comprehensive treatment of publicly available data.

This data analysis is oriented toward the initial stages of the definition of the inherent resource potential of the nodules per se, and their possible use as indicators of other nodule deposits as well as other types of marine mineral resources. Both composite and disaggregated data portrayals presented herein are intended to encourage verification with more recent data and, ultimately, to provide significant substance for quantification of multivariate data relationships to be used in resource appraisal, mineral exploration, and artificial intelligence applications.

Acknowledgements

The author wishes to acknowledge Dr. Allen L. Clark of the East-West Center, Honolulu, Hawaii, for his suggestions and assistance in establishing the extents of the Indian Ocean, Line Islands, and Clarion-Clipperton resource model areas.

Data description

Raw geochemical data were taken directly from McKelvey (1983) who, in turn, retrieved them from the Scripps Institute of Oceanography (SIO) Nodule Data Base (Frazer and Fisk, 1980). Data were prepared by forward transformation of coordinates from geographic to Cartesian coordinates in the Hatano equal area projection (Evenden, 1990).

Figure 1a shows continental boundaries and major ocean bottom geologic features. Figure 1b shows locations of pre-established reference areas and original ungridded data sample sites.

Original data

Approximately 2400 samples from the SIO nodule data bank compose the data used in this study. Depth of sample in meters, sample site coordinates in latitude and longitude, and geochemical analyses for weight-percent of Co, Ni, Mn, Fe, Cu, Zn, Pb, and Si are the variables constituting the unit record of the original raw data set. Presence of longitude, latitude between 60° N. and 65° S., and depth or analytical data for at least one of the above geochemical variables constituted the criteria for retrieval. Not all sample sites have data values for all variables.

Data in this study are intentionally fixed in time to facilitate hypothesis testing involving data captured after circa 1980.

Gridding

The manganese nodule sample data used here have a very low sample density, thereby requiring analysis based on a very small scale spatial distribution and appropriate assumptions regarding spatial continuity of metal content. The continuity assumptions directly influence the gridding process where selectable interpolation parameters are used to control the the area of influence and aggregated value of each cell of the gridded matrix.

After repeated trials of various combinations of grid cell sizes, search radii, and weighting functions, a 200 × 84 grid of squares was superimposed on the geographic extents of the study area (viz., 360° of longitude between 60° N. and 65° S. latitude) and geochemical data were interpolated using a 5 grid cell maximum search radius and a distance function. These parameters seemed to offer the most reasonable balance of data smoothing, filling of open space, and minimum distortion of the original ungridded surface portraying each variable.

Statistical summary

In order to assess properly the distribution patterns for the variables, a brief statistical summary was necessary to determine their numerical attributes such as the mean, median, standard deviation, range, etc. Additionally, the range

Table 1: Descriptive statistics for entire gridded global data distribution.

	Variables									
	Co	Ni	Mn	Fe	Cu	Zn	Pb	Al	Si	Depth
N	5531	5596	5637	5635	5570	3836	3581	2291	1824	5602
$\bar{X}$	0.25	0.52	16.70	13.68	0.30	0.12	0.10	2.82	7.86	4.14
σ^2	0.02	0.07	22.87	13.08	0.05	0.05	0.00	0.78	6.15	0.74
σ	0.13	0.26	4.78	3.62	0.22	0.21	0.05	0.88	2.48	0.86
X_{low}	0.01	0.01	0.26	3.60	0.01	0.00	0.00	0.52	1.70	0.76
X_{high}	1.27	1.53	34.06	32.97	1.22	3.43	0.33	7.51	20.08	7.09
ΔX	1.26	1.52	33.80	29.37	1.21	3.43	0.33	6.99	18.38	6.33
Class numbers										
10^{th}	0.12	0.23	11.43	9.23	0.11	0.05	0.05	1.74	5.19	2.98
20^{th}	0.15	0.30	13.12	10.65	0.14	0.06	0.06	2.14	5.96	3.45
30^{th}	0.18	0.36	14.16	11.75	0.16	0.06	0.08	2.39	6.52	3.73
40^{th}	0.21	0.40	15.07	12.62	0.19	0.07	0.09	2.60	6.91	4.02
50^{th}	0.23	0.46	16.10	13.57	0.23	0.07	0.10	2.76	7.38	4.23
60^{th}	0.25	0.51	17.02	14.44	0.29	0.08	0.11	2.97	7.93	4.46
70^{th}	0.29	0.59	18.28	15.48	0.34	0.10	0.12	3.20	8.61	4.68
80^{th}	0.34	0.70	20.06	16.82	0.42	0.12	0.14	3.41	9.65	4.91
90^{th}	0.42	0.92	23.24	18.37	0.60	0.15	0.16	3.77	11.47	5.15
95^{th}	0.50	1.08	26.07	19.53	0.81	0.28	0.18	4.36	12.76	5.34

was divided into 100 equal sized classes where the first class contains the lowest data values. Descriptive statistics for every 10^{th} class plus the 95^{th} class are presented in Table 1.

Percentiles could have been used and would have been effective transformations, but the transformations would have constituted one additional step removed from the data. In this case it is felt that data class boundaries are more appropriate as a "first pass" data review. Of course, this does not intend to preclude use of percentiles or any other useful data transformation when deemed appropriate by another investigator.

Class number is a simplistic method of normalizing multiple variables so that their frequency and spatial distributions can be compared without necessity of continued reference to their individual frequency distribution attributes in weight-percent or meters of depth.

Pre-selected model areas

In addition to continental boundaries, four relatively small areas of grid cells are plotted on all maps. These areas are used as bases of geographic and geologic reference with the spatial distributions of the variables.

The easternmost of these is a cell cluster representing the zone bounded on the north and south by the Clarion and Clipperton fault zones, respectively, and is commonly referred to as the Clarion-Clipperton Zone. This area is presented as an area of reference because of its high nodule sampling density and high nickel, copper, and manganese content.

The two almost contiguous cell clusters that bound the western side of the Clarion-Clipperton Zone collectively represent the Line Islands area, and were selected because of high nodule content of nickel and copper, and low iron content.

The westernmost cluster is an area central to the Indian Ocean, and was selected principally because of the presence of nodules having high content of nickel, copper, and manganese and, at this time, it appears to be the largest single metal-enriched area of contiguous grid cells in oceans of the eastern hemisphere.

Spatial distributions

Spatial distributions of variables are herein portrayed graphically in two ways; (1) as conventional composite grey-level maps (Botbol 1989, 1990) where grey-levels correspond to six concentration ranges expressed as class number ranges, and (2) as sets of six maps, one map for the distribution of each concentration range in its companion composite map. The latter are referred to as disaggregated maps and are accompanied by contracted verbal descriptions of the spatial distributions of each variable presented in tabular form.

Composite maps

Each variable is portrayed by grey levels that correspond to the following fixed set of six class number ranges; 1^{st} - 10^{th}, 11^{th} - 30^{th}, 31^{st} - 50^{th}, 51^{st} - 70^{th}, 71^{st} - 90^{th}, and 91^{st} - 100^{th}. These class number ranges are the same for all composite maps and provide an adequate very small scale view of the global distributions of the variables.

Disaggregated maps

For each grey-level on the composite maps there is a separate map of the spatial distribution of that particular grey-level. Cells occuring within the stated class number range are colored black, and other areas having data at other class number ranges are light grey. In this way, the spatial relationships between each of the class number ranges can be rapidly visually correlated with other class number ranges, geologic, geographic, and other geochemical variables. In many cases there are distinct zoning patterns such as halos and linears that are present in the disaggregated maps and are present but obscured in the composite maps.

The technique of disaggregated map portrayal, particularly in an interactive computer graphics environment, appears to be a valuable interpretation tool. The maps can be composed and intersected simply and rapidly, and provide a data filter that optimizes interpretation.

Maps and comments

This section presents index, composite and disaggregated maps as well as contracted descriptions of the variables represented in the disaggregated maps. The reader is reminded that each disaggregated map represents one class number interval on its companion composite map. Since there are six intervals in the

composite maps, each interval is represented by one of six single disaggregated maps.

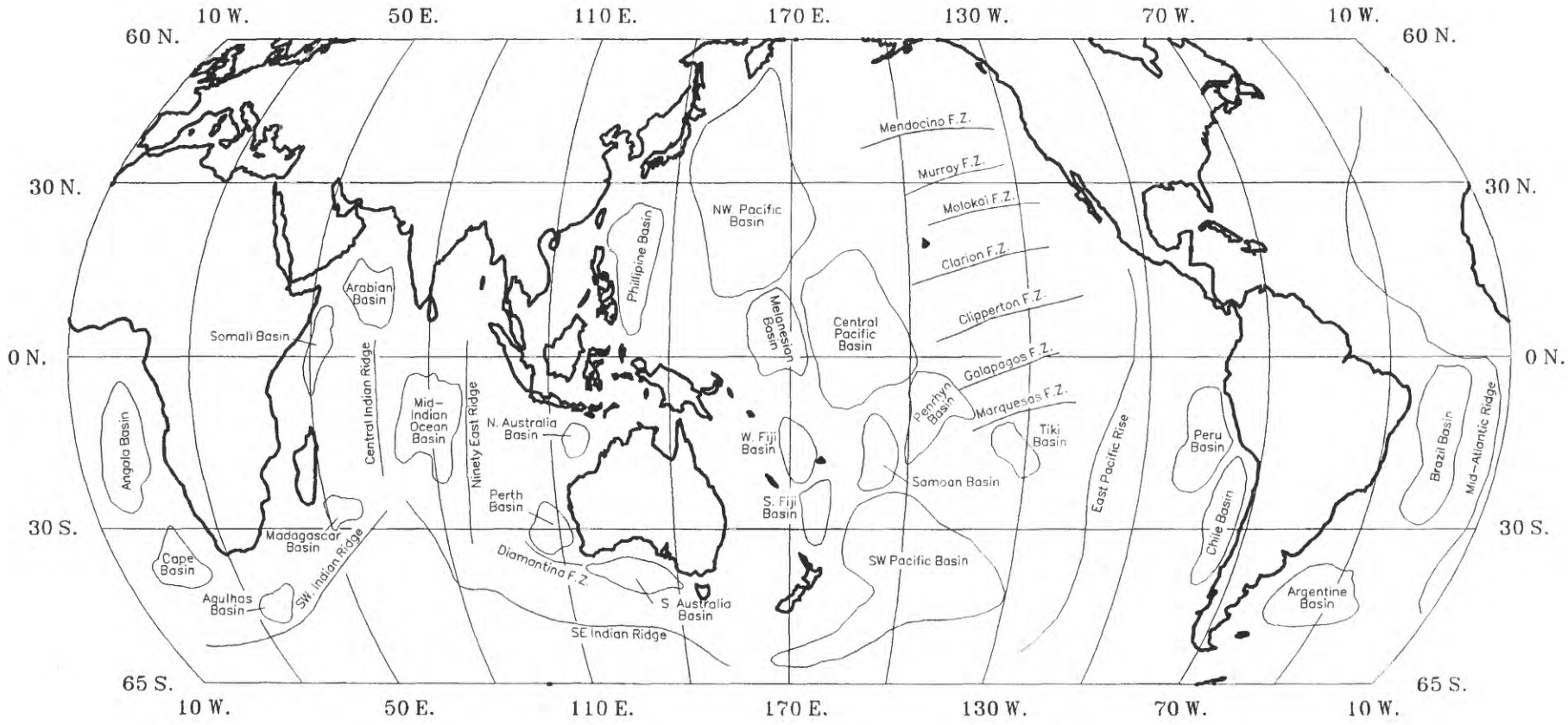

Figure 1a. Index map of continents and major ocean bottom geologic features.

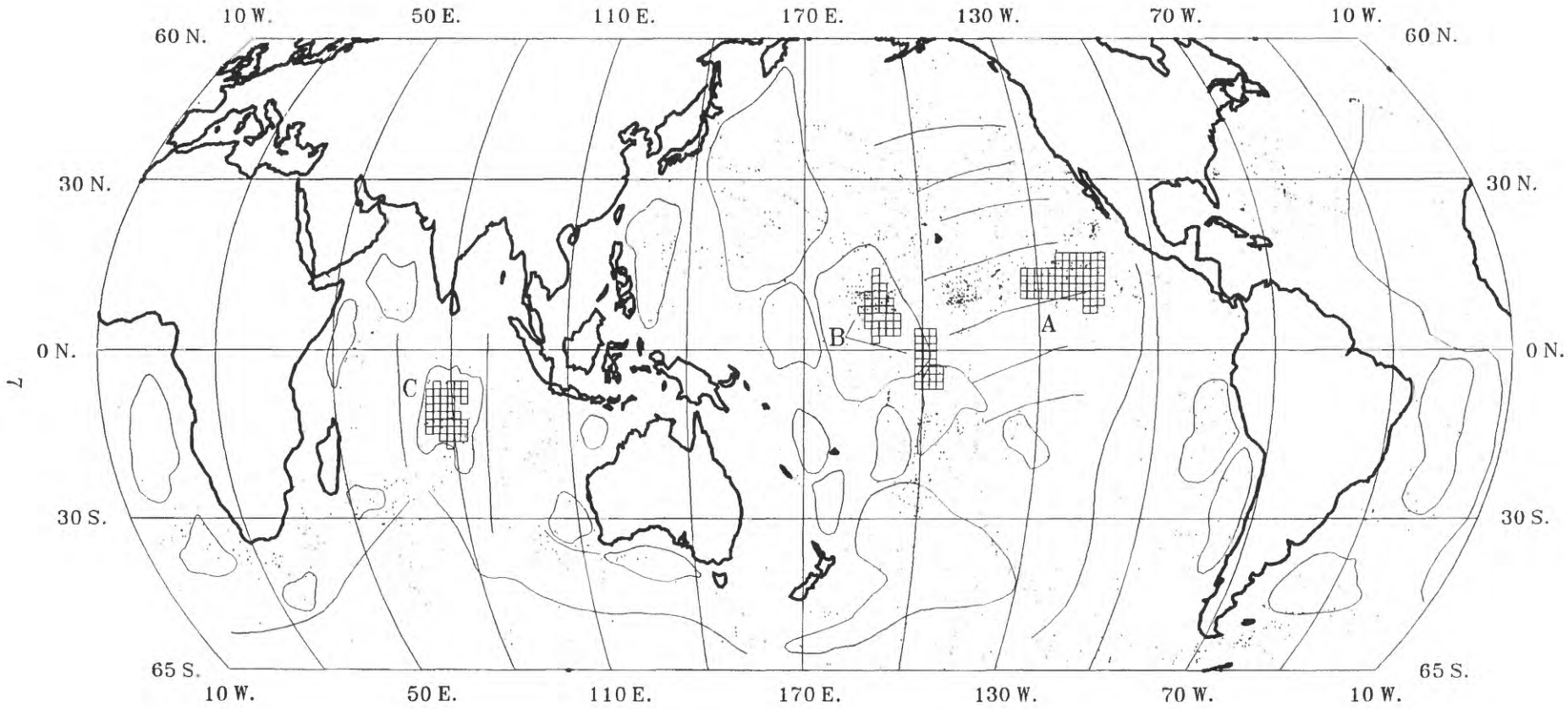

Figure 1b. Index map of coastlines, major ocean bottom geologic features, sample sites, and model areas A (Clarion-Clipperton), B (Line Islands), and C (Indian Ocean).

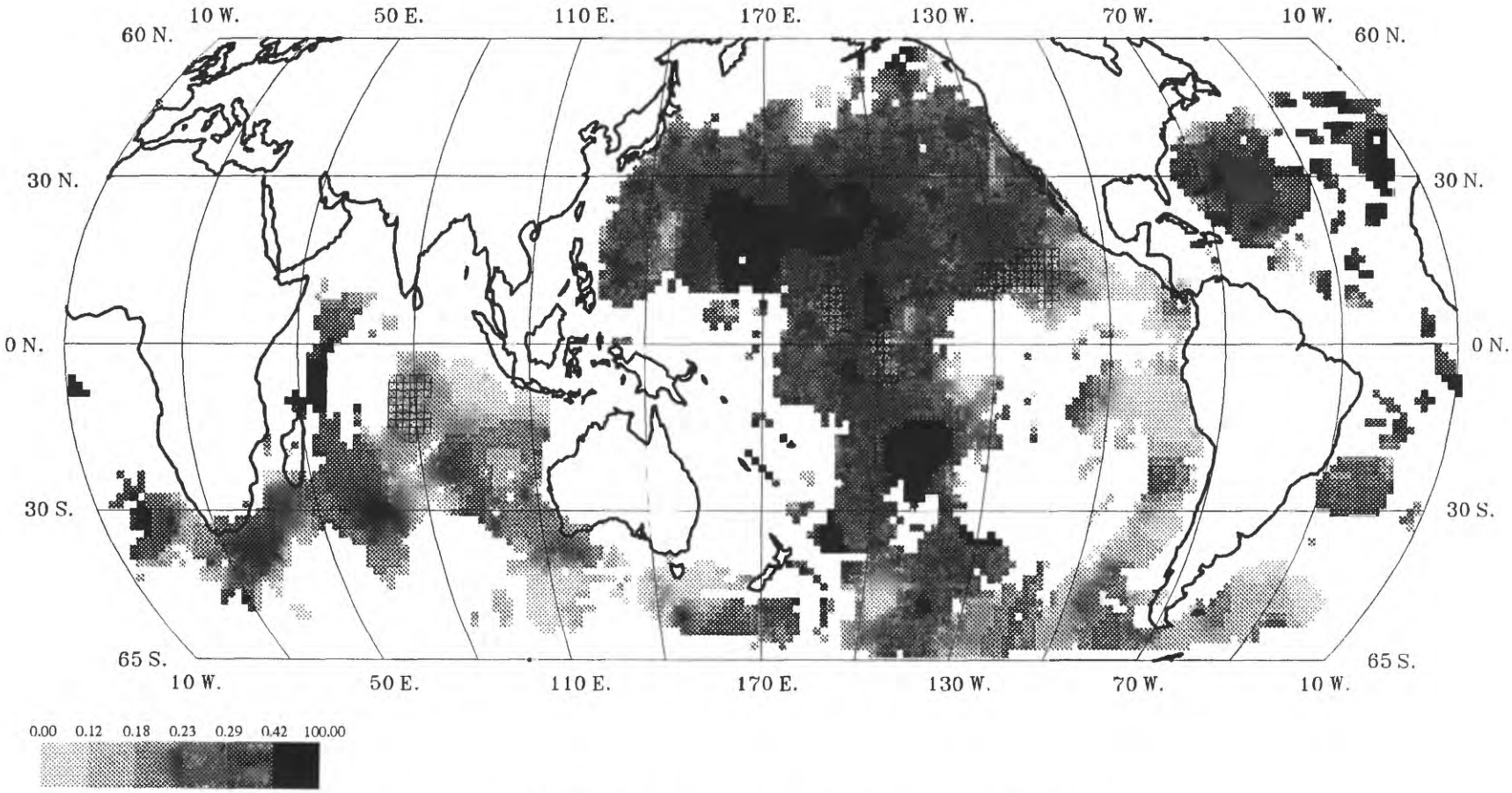

Figure 2a. Distribution of Co (weight percent) in manganese nodules.

Grey level boundaries represent data values for class numbers 1, 10, 30, 50, 70, 90, and 100.

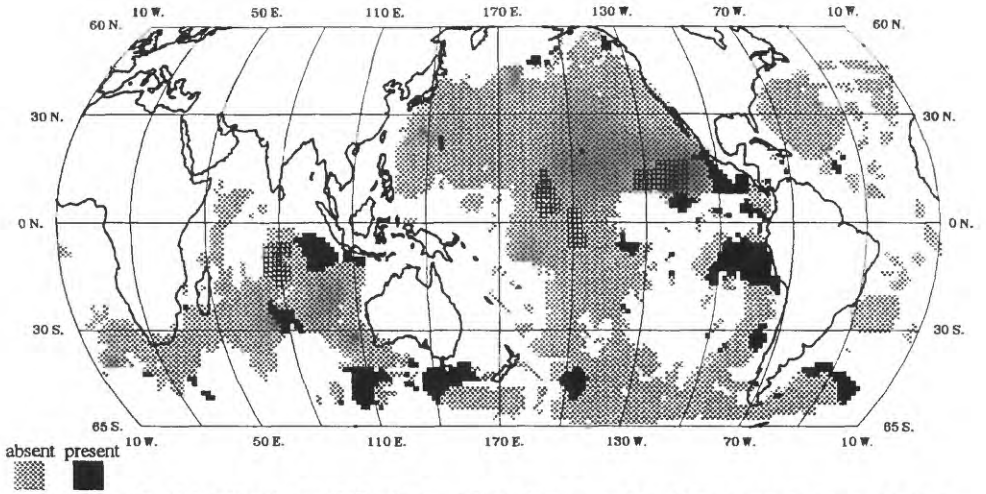

Figure 2b. Distribution of Co (1st - 10th class numbers) in manganese nodules.

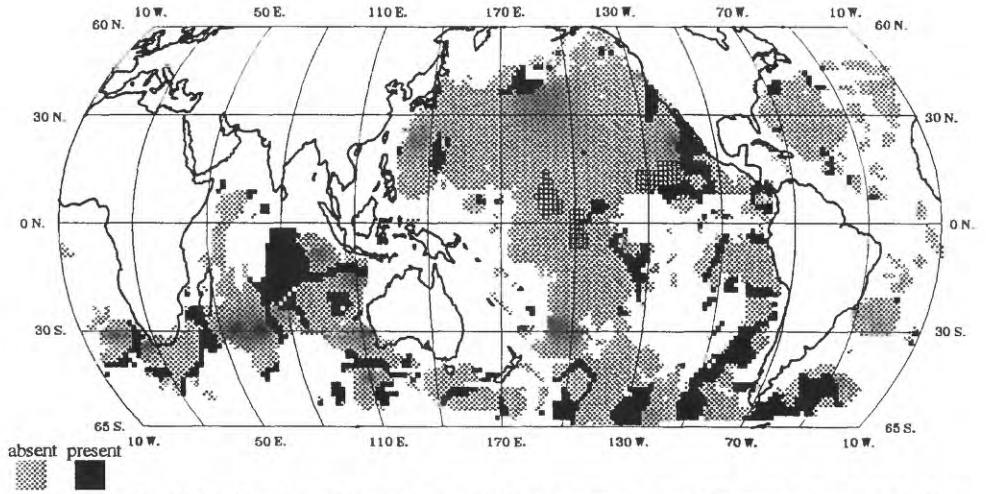

Figure 2c. Distribution of Co (11th - 30th class numbers) in manganese nodules.

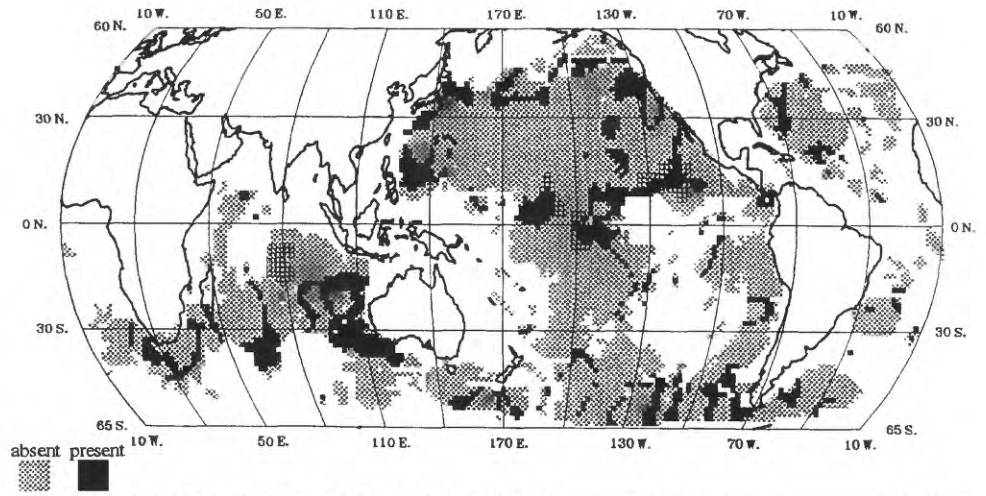

Figure 2d. Distribution of Co (31st - 50th class numbers) in manganese nodules.

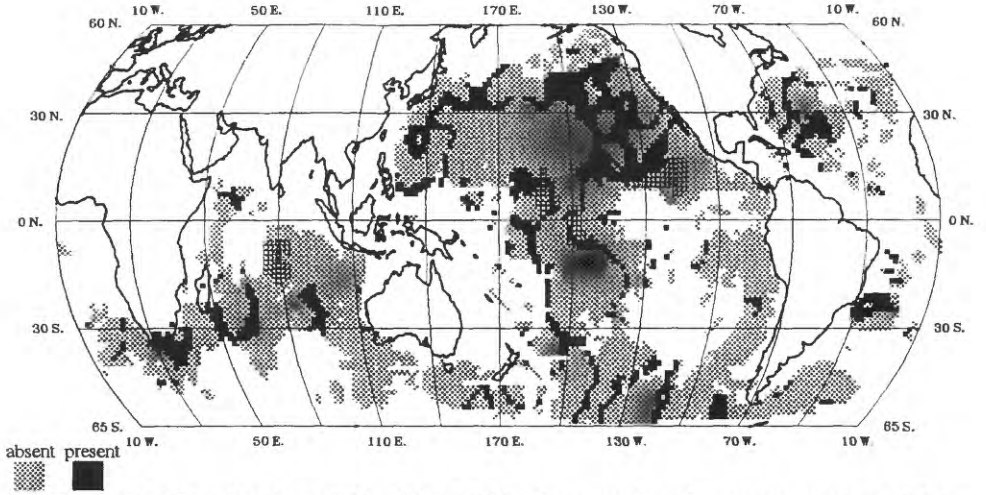

Figure 2e. Distribution of Co (51st - 70th class numbers) in manganese nodules.

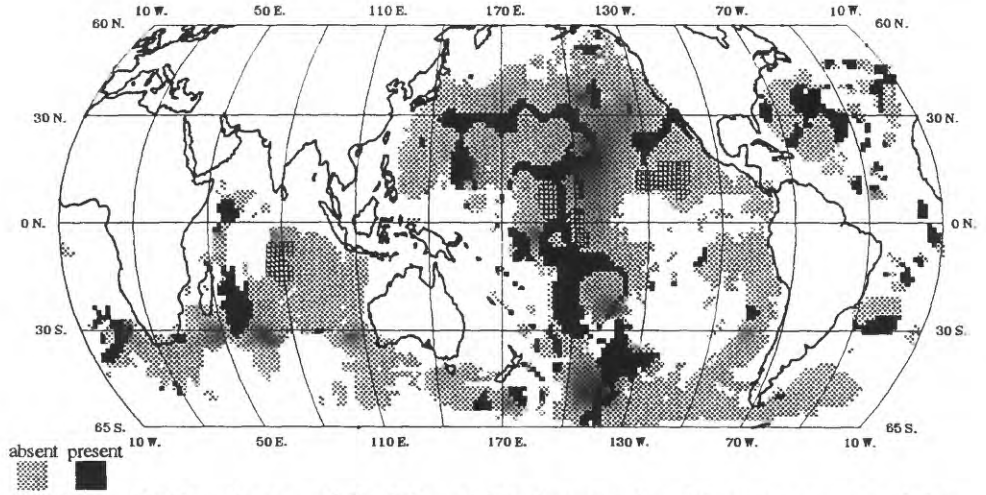

Figure 2f. Distribution of Co (71st - 90th class numbers) in manganese nodules.

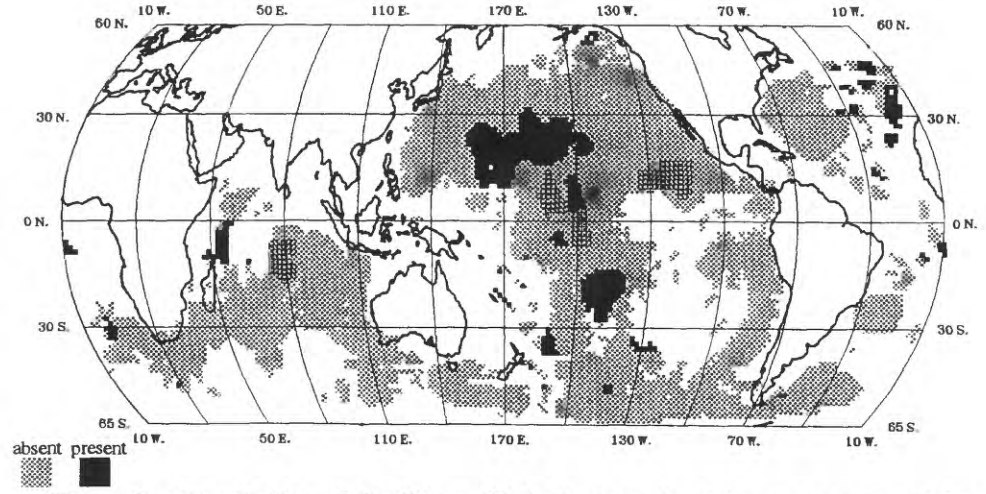

Figure 2g. Distribution of Co (91st - 100th class numbers) in manganese nodules.

Table 2: Salient features of the disaggregated **Co** spatial distribution.

Variable	Comments
1^{st} – 10^{th} class numbers	A large cluster occurs in the Peru Basin. Scattered small-medium clusters occur mostly in the southern latitudes. A small cluster intersects the southern tip of the Clarion-Clipperton model.
11^{th} – 30^{th} class numbers	The Indian Ocean model is completely covered. Remaining positive areas are mostly in the southern latitudes and consist of small-medium clusters, northeast and northwest trending linears, and vestigial halos.
31^{st} – 50^{th} class numbers	≈50% of the Line Islands and Clarion-Clipperton models are covered. Complete cover of the Perth Basin. Small-medium clusters form a very large vestigial halo in Northern Pacific. Remaining positive areas are widely scattered small-medium clusters, linears, and vestigial halos.
51^{st} – 70^{th} class numbers	≈20% of the Line Islands and the Clarion-Clipperton models are covered. Large north trending trio of contiguous halos covers Clarion through Mendocino Fault Zones. Contraction and better definition of large halo in the northern circum-Pacific. Remaining occurrences are widely scattered thin linear clusters and vestigial halos.
71^{st} – 90^{th} class numbers	A very large cluster intersects the Samoan, Penrhyn, and Southwest Pacific basins. The halo north of the Line Islands model is contracted and better defined. A large north trending cluster extends from 65°S. to 30°S. and intersects the Southwest Pacific Basin. A southeast trending medium cluster intersects the Mid-Atlantic Ridge at ≈30°N. Medium clusters intersect the Brazil, Madagascar, and Cape Basins. Remaining clusters are small-medium and widely scattered.
91^{st} – 100^{th} class numbers	A very large cluster occurs north of the Line Islands model. A small cluster occurs east of the northern part of the Line Islands model. A medium cluster occurs between the Penrhyn and Southwest Pacific basins. The few remaining clusters are small-medium and widely scattered.

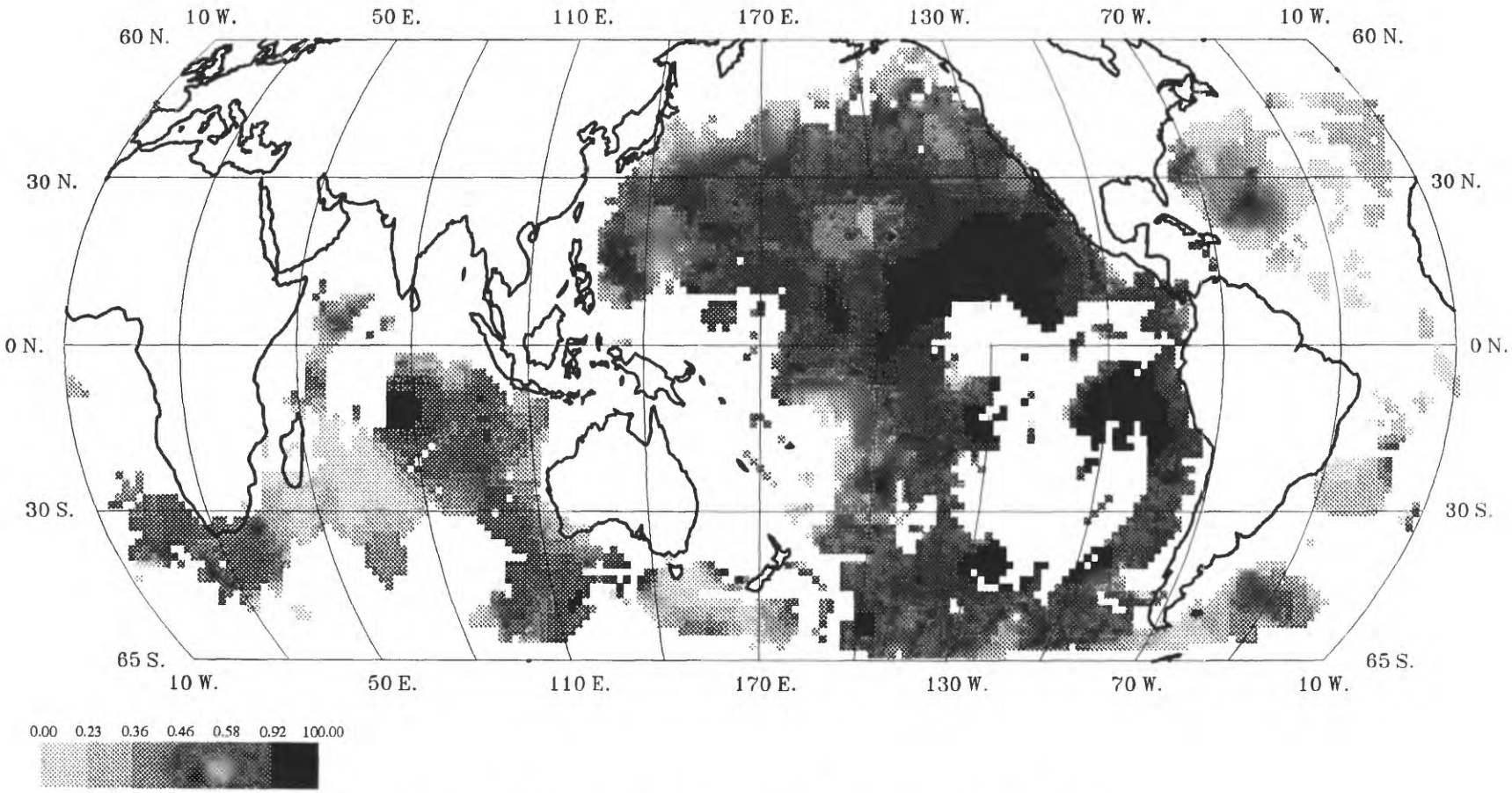

Figure 3a. Distribution of Ni (weight percent) in manganese nodules.

Grey level boundaries represent data values for class numbers 1, 10, 30, 50, 70, 90, and 100.

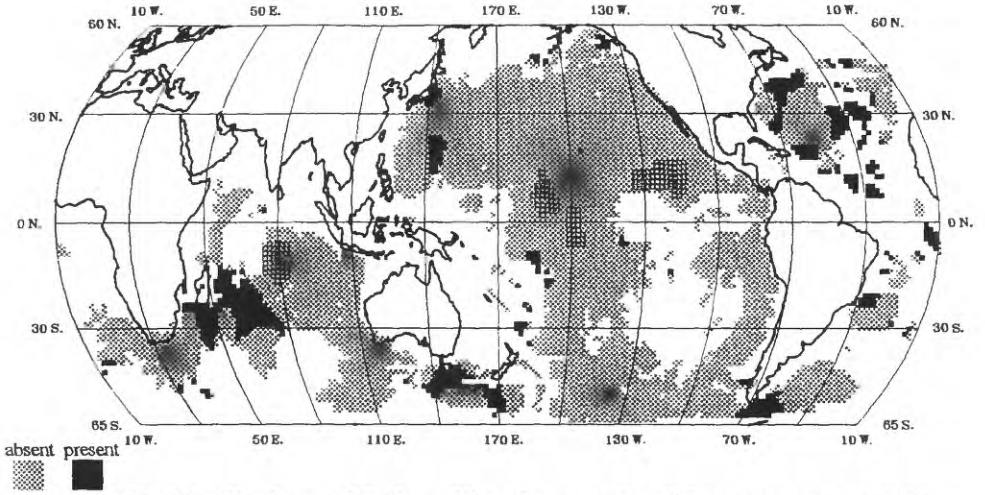

Figure 3b. Distribution of Ni (1st - 10th class numbers) in manganese nodules.

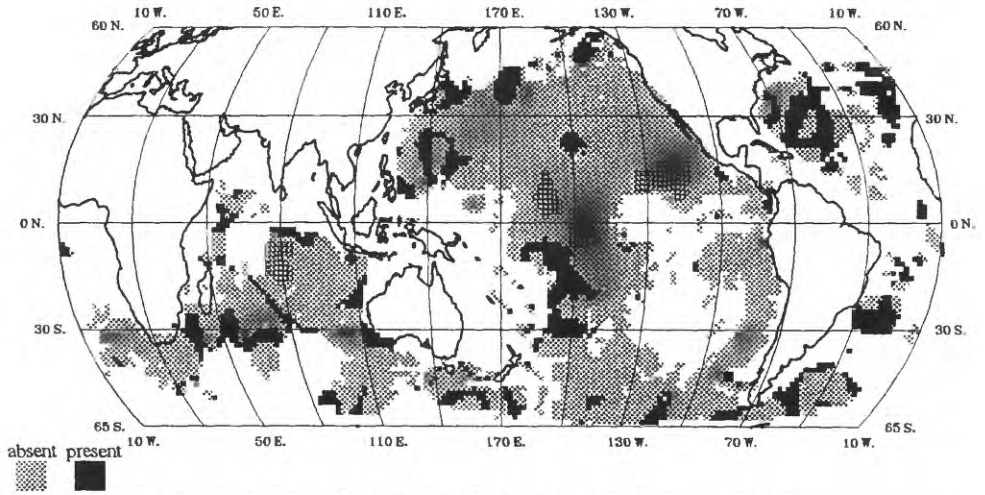

Figure 3c. Distribution of Ni (11th - 30th class numbers) in manganese nodules.

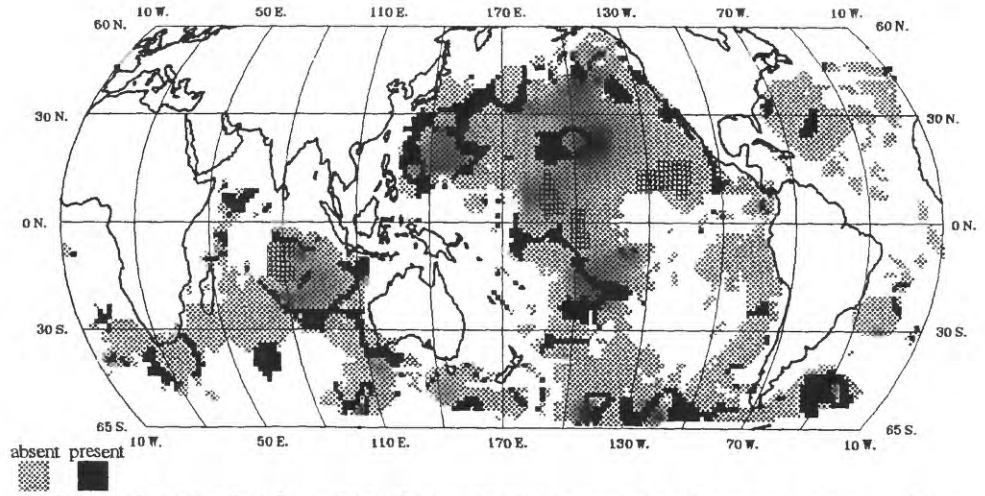

Figure 3d. Distribution of Ni (31st - 50th class numbers) in manganese nodules.

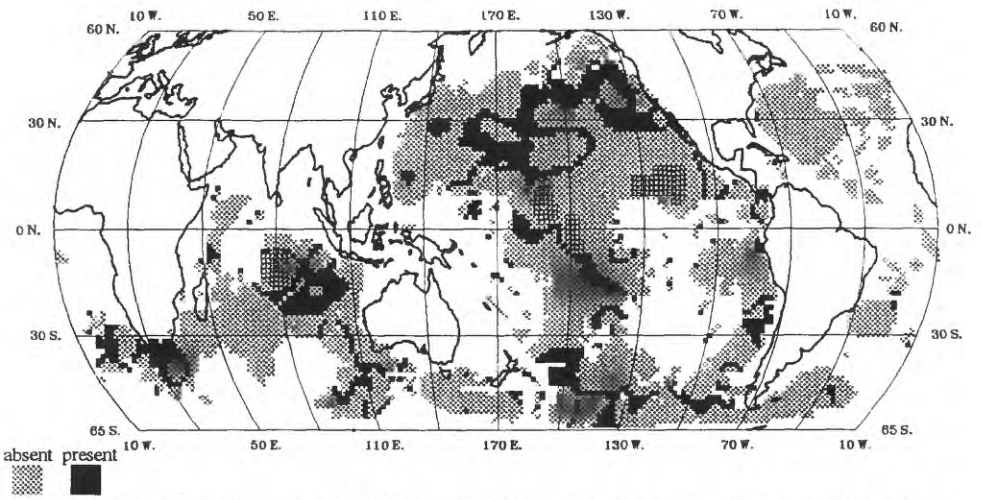

Figure 3e. Distribution of Ni (51st - 70th class numbers) in manganese nodules.

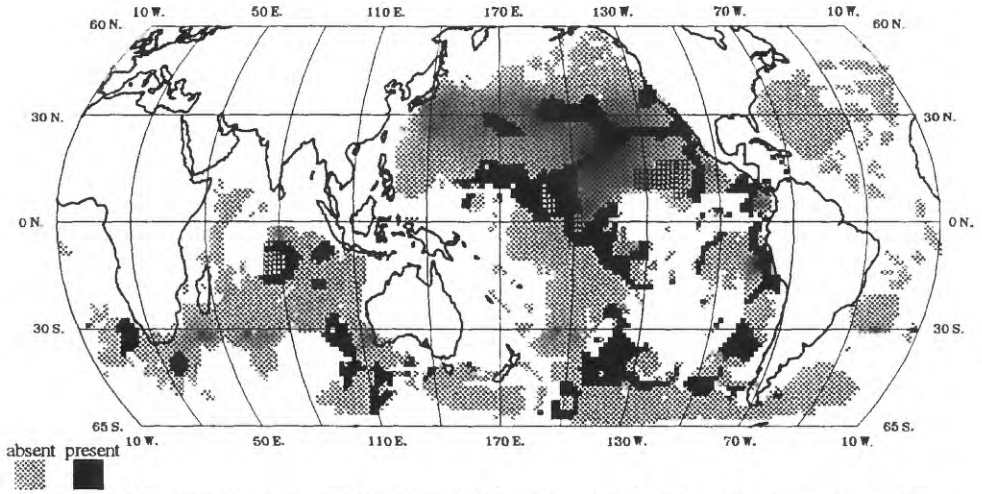

Figure 3f. Distribution of Ni (71st - 90th class numbers) in manganese nodules.

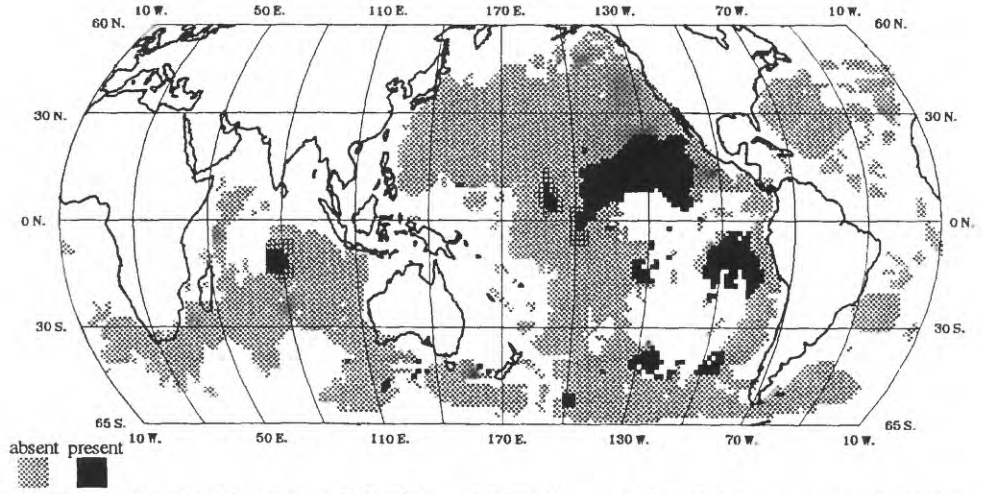

Figure 3g. Distribution of Ni (91st - 100th class numbers) in manganese nodules.

Table 3: Salient features of the disaggregated **Ni** spatial distribution.

Variable	Comments
1^{st} – 10^{th} class numbers	Medium-large clusters occur south and east of Madagascar. The remaining clusters are mostly small and widely scattered.
11^{th} – 30^{th} class numbers	Large clusters occur south of the Line Islands model, and a large halo occurs in the north Atlanic between 70°W. and 40°W The remaining clusters are small-medium and widely scattered. There is a north-west trending thin linear south of the Indian Ocean model.
31^{st} – 50^{th} class numbers	This distribution shows mostly widely scattered small-large linear halos and vestiges of halos. An arcuate linear pattern occurs south of the Indian Ocean model.
51^{st} – 70^{th} class numbers	Halos are generally contracted relative to those of lower concentrations, particularly in the northern Pacific. A large cluster occurs southeast of the Indian Ocean model.
71^{st} – 90^{th} class numbers	A well-defined very large semi-continuous halo occurs around the Clarion-Clipperton model, intersects the Line Islands model, and forms the northern part of a major semi-continuous halo in the eastern Pacific from 40°N to 60°S. A small halo partially encloses the Indian Ocean model.
91^{st} – 100^{th} class numbers	A very large cluster covers the Clarion-Clipperton model and part of the Line Islands model. A small cluster intersects the central Indian Ocean model.

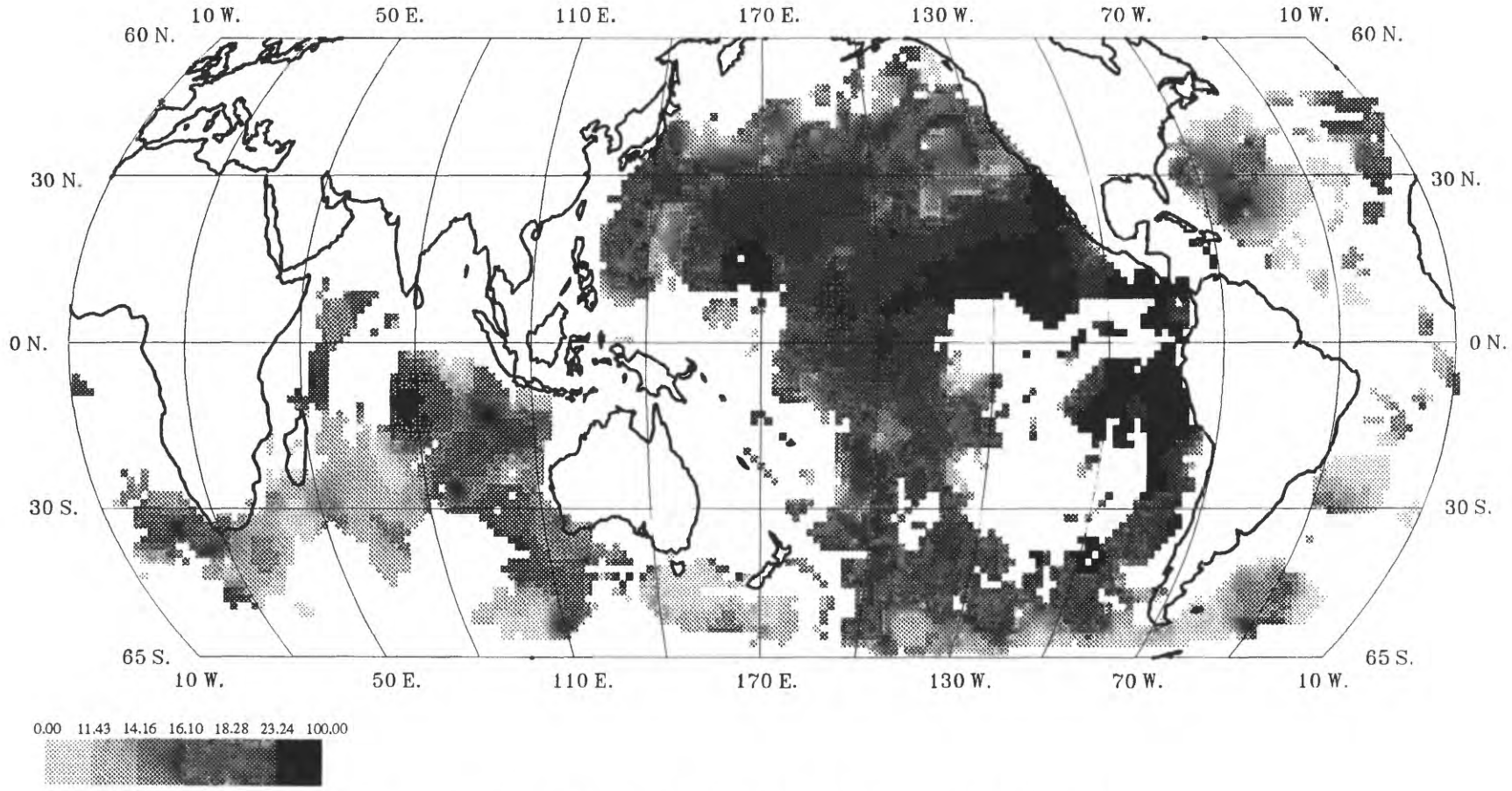

Figure 4a. Distribution of Mn (weight percent) in manganese nodules.

Grey level boundaries represent data values for class numbers 1, 10, 30, 50, 70, 90, and 100.

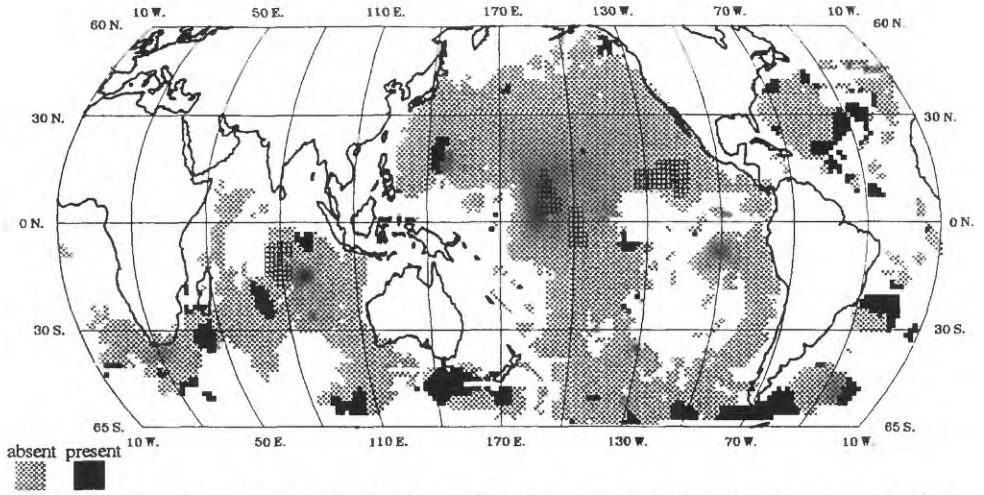

Figure 4b. Distribution of Mn (1st - 10th class numbers) in manganese nodules.

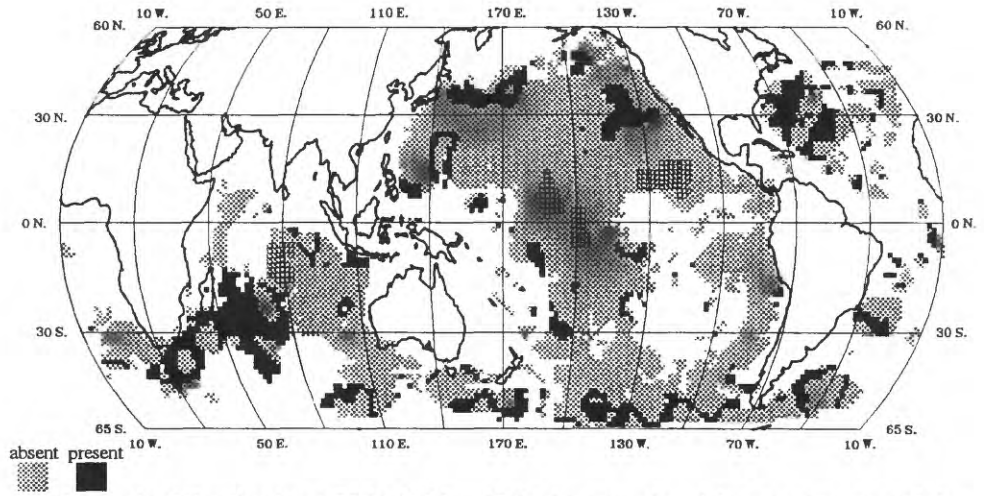

Figure 4c. Distribution of Mn (11th - 30th class numbers) in manganese nodules.

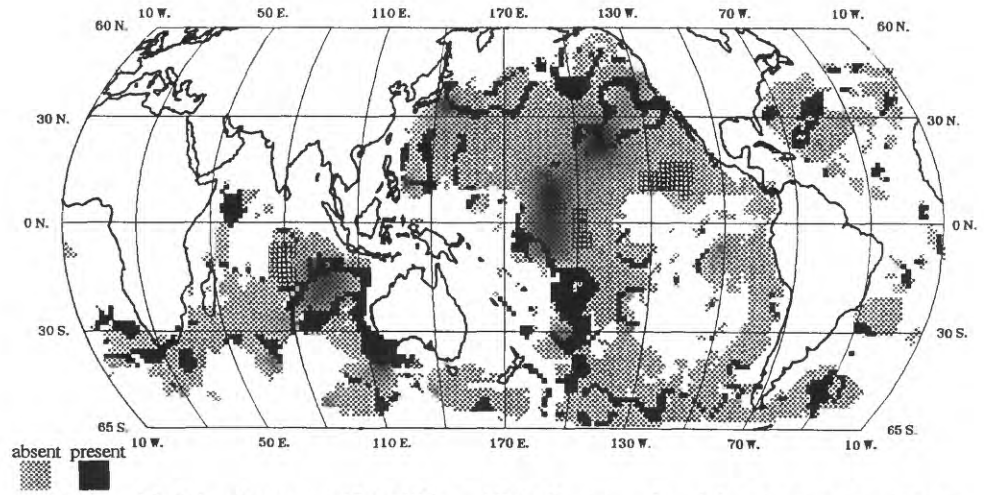

Figure 4d. Distribution of Mn (31st - 50th class numbers) in manganese nodules.

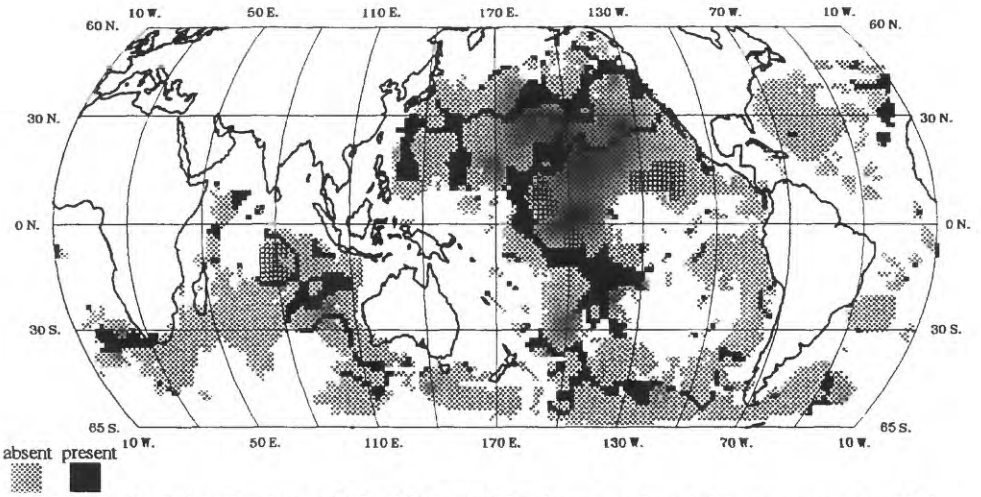

Figure 4e. Distribution of Mn (51st - 70th class numbers) in manganese nodules.

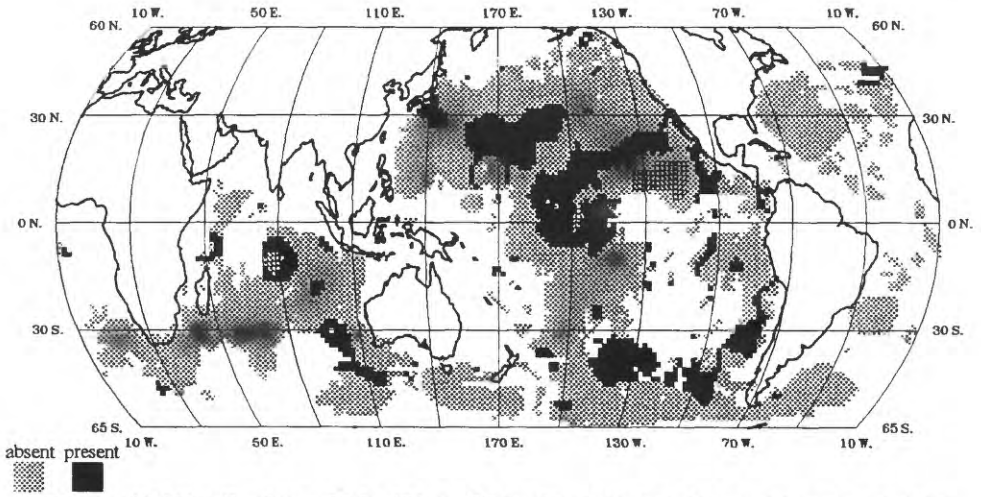

Figure 4f. Distribution of Mn (71st - 90th class numbers) in manganese nodules.

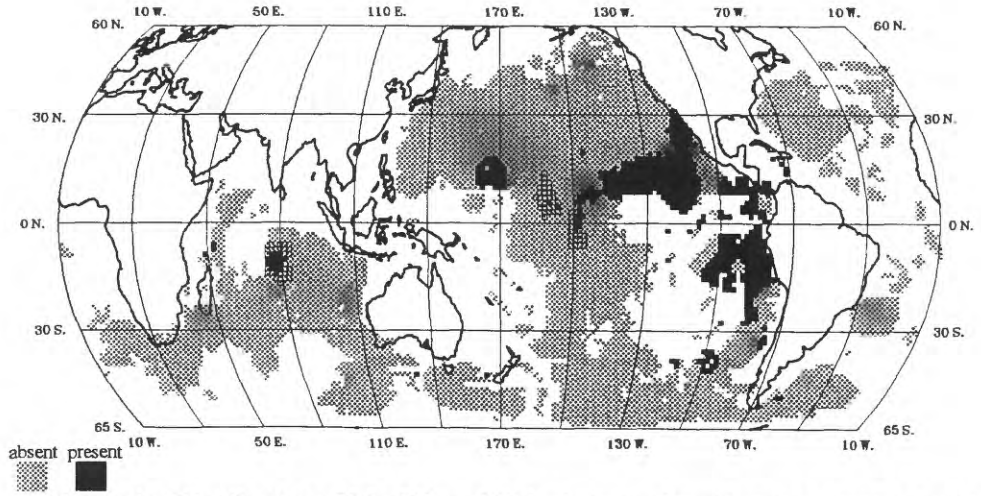

Figure 4g. Distribution of Mn (91st - 100th class numbers) in manganese nodules.

Table 4: Salient features of the disaggregated **Mn** spatial distribution.

Variable	Comments
1^{st} – 10^{th} class numbers	This concentration range is characterized by a few widely scattered small-medium clusters.
11^{th} – 30^{th} class numbers	A large cluster occurs southwest of the Indian Ocean model. A semi-continuous east trending linear occurs at $\approx 60°$S, from 160°W. to 15°W. The remaining clusters are small-medium and widely scattered.
31^{st} – 50^{th} class numbers	The vestige of a very large zone of halos occurs in the circum North Pacific. A large cluster covers the Perth and South Australia basins, and Diamantina Fracture Zone. A medium halo occurs southeast of the Indian Ocean model. A large north trending cluster extends from $\approx 60°$S. to $\approx 10°$S. intersecting Samoan, Penrhyn, and northern Southwest Pacific basins.
51^{st} – 70^{th} class numbers	The southeast boundaries of a well defined trio of large east trending northern Pacific halos form the northern part of a large halo west of and intersecting the Line Islands model. There is a thin halo around the Indian Ocean model, and a thin east trending irregular linear at 60°S from 160°W to 70°W.
71^{st} – 90^{th} class numbers	A very large cluster occurs northwest of the Line Islands model. A very large discontinuous halo covers the Line Islands model and encloses the northern Clarion-Clipperton model. A small halo encloses most of the Indian Ocean model. A small linear occurs southwest of Diamantina Fracture Zone. A large arcuate cluster group in the circum-southeast Pacific intersects the Chile Basin, the southern axis of the East Pacific Rise, and the Southwest Pacific Basin.
91^{st} – 100^{th} class numbers	A small cluster is centered in the Indian Ocean model. A small cluster intersects Melanesian and Northwest Pacific basins. A very large massive cluster covers the Clarion-Clipperton model and intersects the southern part of the Line Islands model. A large cluster covering the Peru Basin.

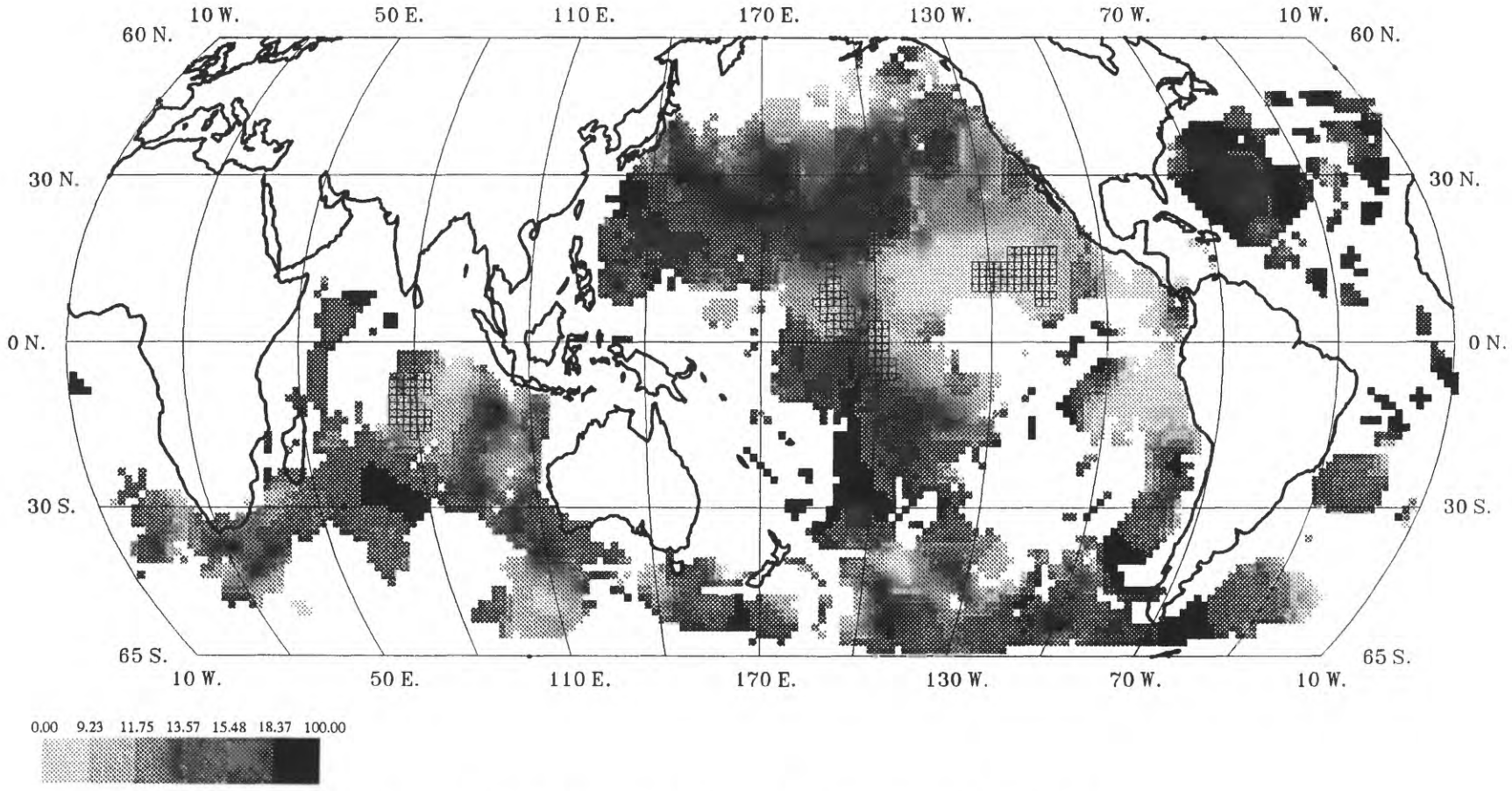

Figure 5a. Distribution of Fe (weight percent) in manganese nodules.

Grey level boundaries represent data values for class numbers 1, 10, 30, 50, 70, 90, and 100.

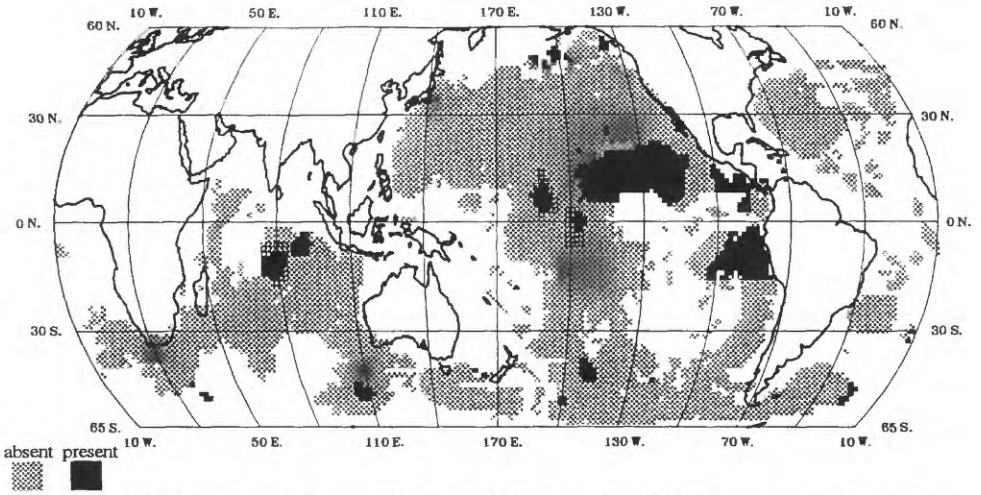

Figure 5b. Distribution of Fe (1st - 10th class numbers) in manganese nodules.

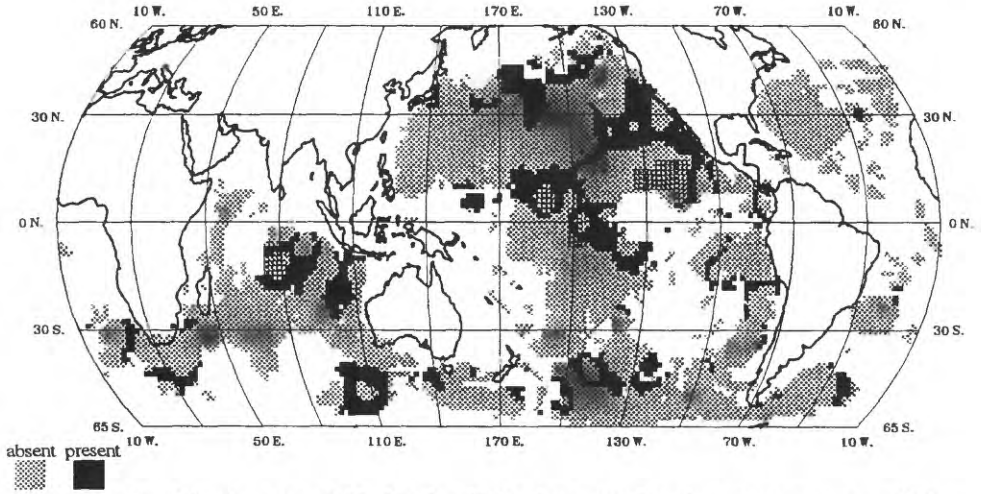

Figure 5c. Distribution of Fe (11th - 30th class numbers) in manganese nodules.

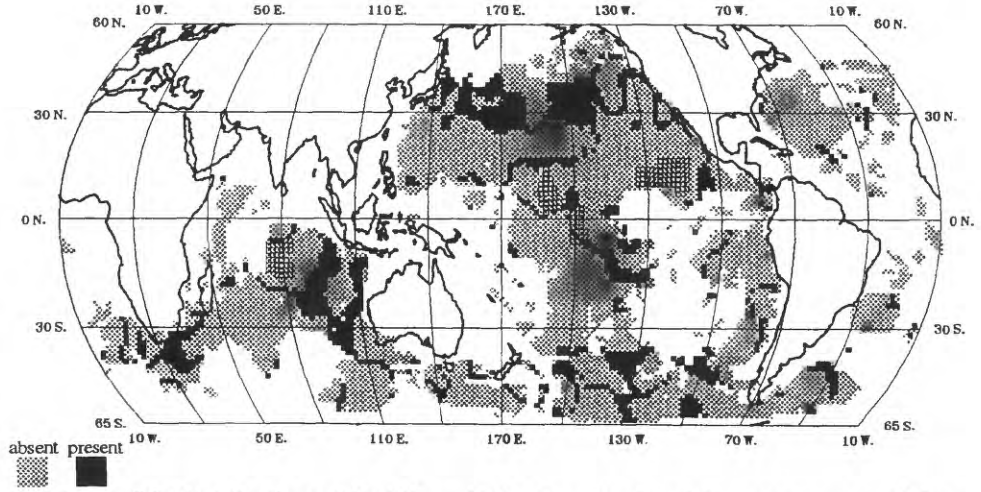

Figure 5d. Distribution of Fe (31st - 50th class numbers) in manganese nodules.

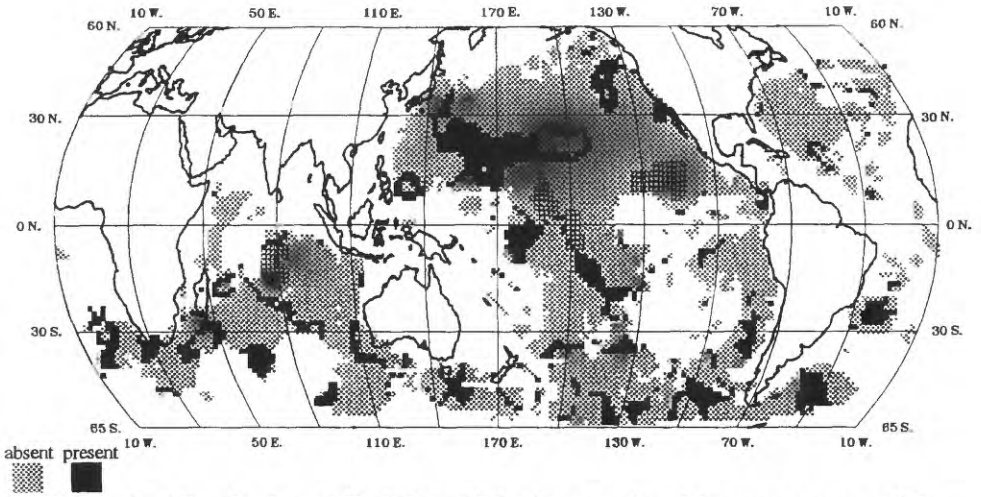

Figure 5e. Distribution of Fe (51st - 70th class numbers) in manganese nodules.

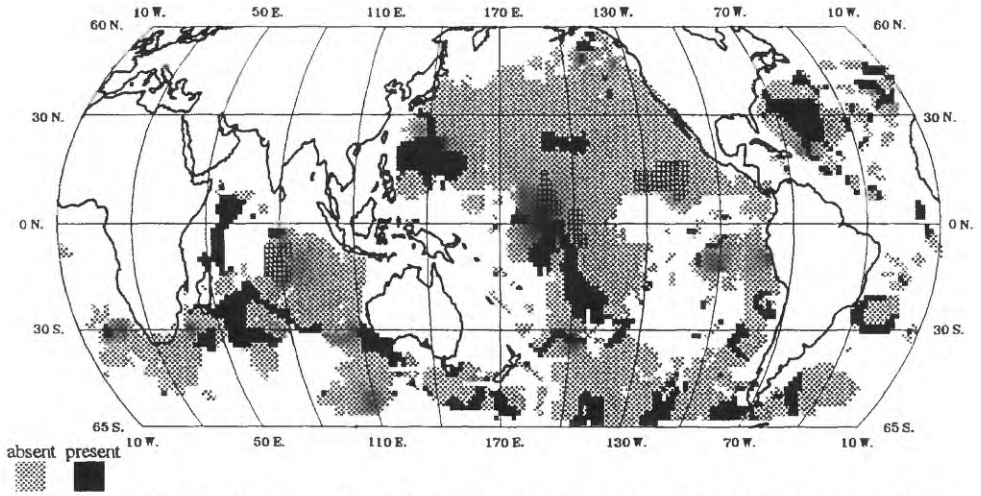

Figure 5f. Distribution of Fe (71st - 90th class numbers) in manganese nodules.

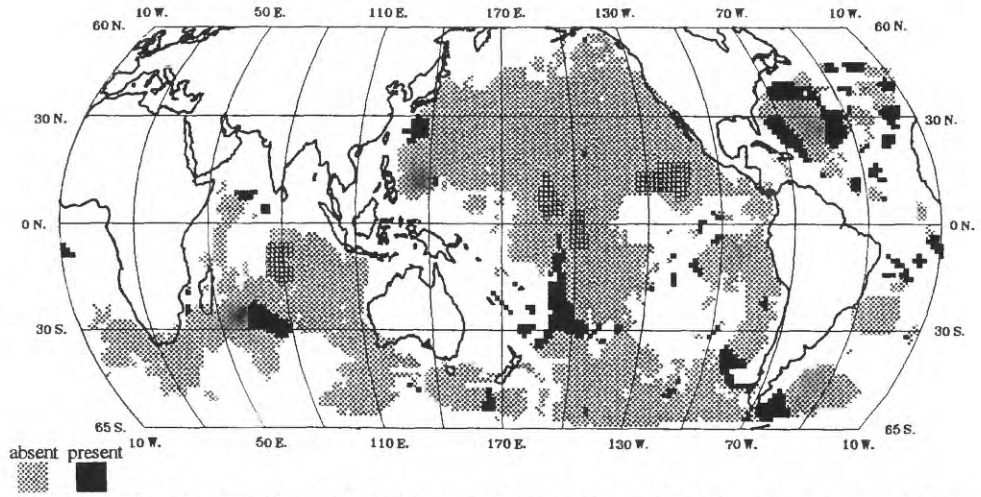

Figure 5g. Distribution of Fe (91st - 100th class numbers) in manganese nodules.

Table 5: Salient features of the disaggregated **Fe** spatial distribution.

Variable	Comments
1^{st} – 10^{th} class numbers	A large cluster covers Peru Basin. A very large cluster covers the Clarion-Clipperton model. There are two small clusters, one in each part of the Line Islands model. A small cluster occurs in the Indian Ocean model. There are very few remaining clusters, all small and widely scattered.
11^{th} – 30^{th} class numbers	Medium halos enclose each part of the Line Islands model and compose the southwestern part of a larger halo that surrounds the Clarion-Clipperton model. A group of medium clusters occurs in north Central Pacific Basin. A small halo encloses the Indian Ocean model.
31^{st} – 50^{th} class numbers	An irregular band of large east trending clusters occur across the northern Pacific. There are two north trending medium clusters east of the Indian Ocean model. The remaining clusters and linears are small and widely scattered.
51^{st} – 70^{th} class numbers	A large east trending cluster occurs north of the Line Islands model and intersects the Northwest Pacific Basin. Remaining clusters and linears are small-medium and widely scattered in southern latitudes.
71^{st} – 90^{th} class numbers	A medium cluster covers Madagascar Basin. A medium north trending linear occurs north of Madagascar. A large cluster intersects the Phillipine and Northwest Pacific Basins. A large north trending linear cluster occurs south of the Line Islands model. A large cluster occurs in the Atlantic, east of Florida, and a medium discontinuous halo occurs east of Brazil.
91^{st} – 100^{th} class numbers	A medium cluster occurs at the intersection of the Southwest and Southeast Indian Ridges. Two medium clusters occur northwest of and east of, respectively, the southern tip of South America. A large discontinuous halo occurs in Atlantic east of Florida. A medium north trending zone south of the Line Islands model intersects the Southwest Pacific Basin and covers the Samoan Basin.

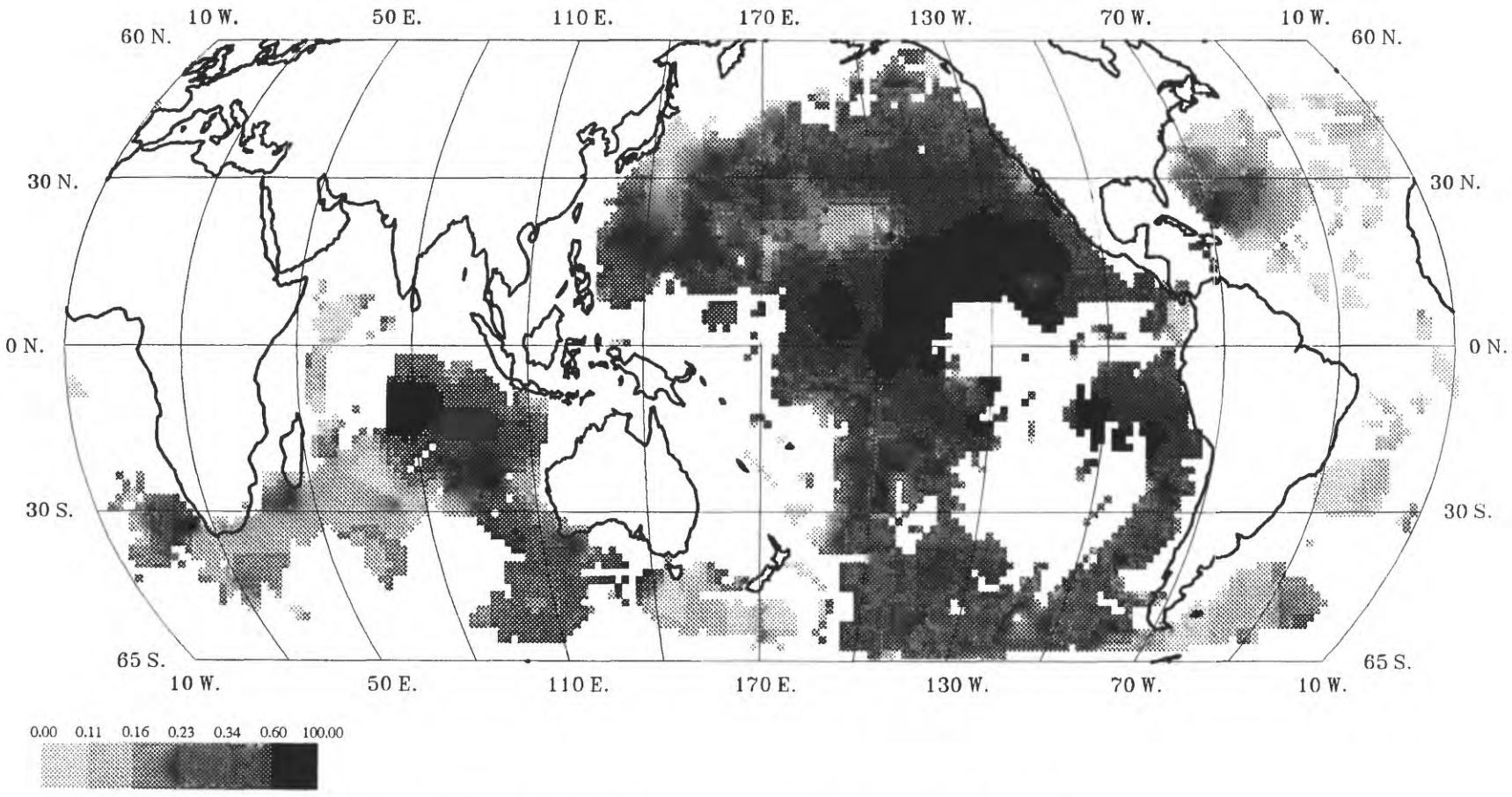

Figure 6a. Distribution of Cu (weight percent) in manganese nodules.

Grey level boundaries represent data values for class numbers 1, 10, 30, 50, 70, 90, and 100.

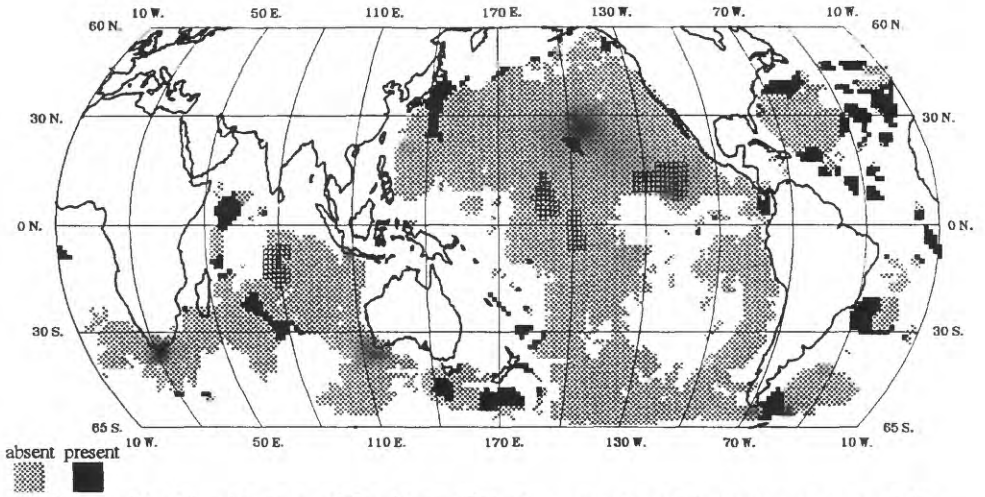

Figure 6b. Distribution of Cu (1st - 10th class numbers) in manganese nodules.

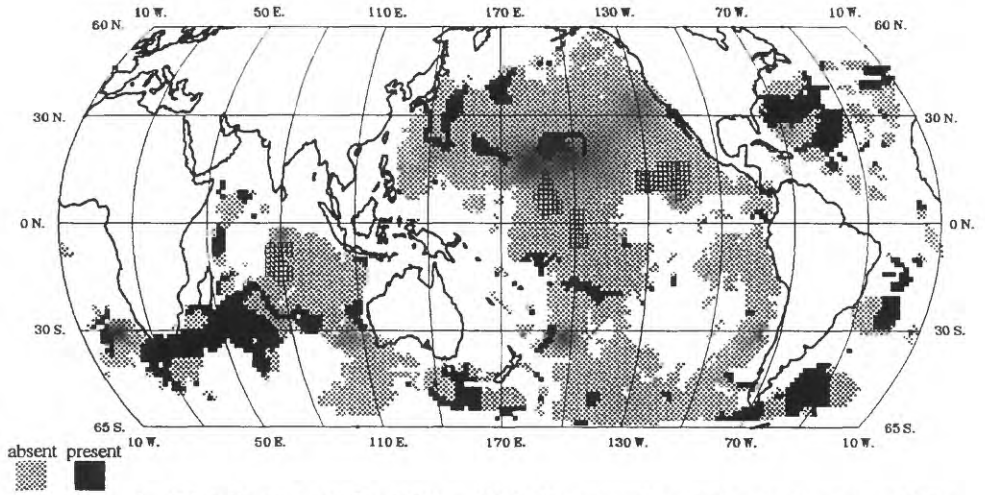

Figure 6c. Distribution of Cu (11th - 30th class numbers) in manganese nodules.

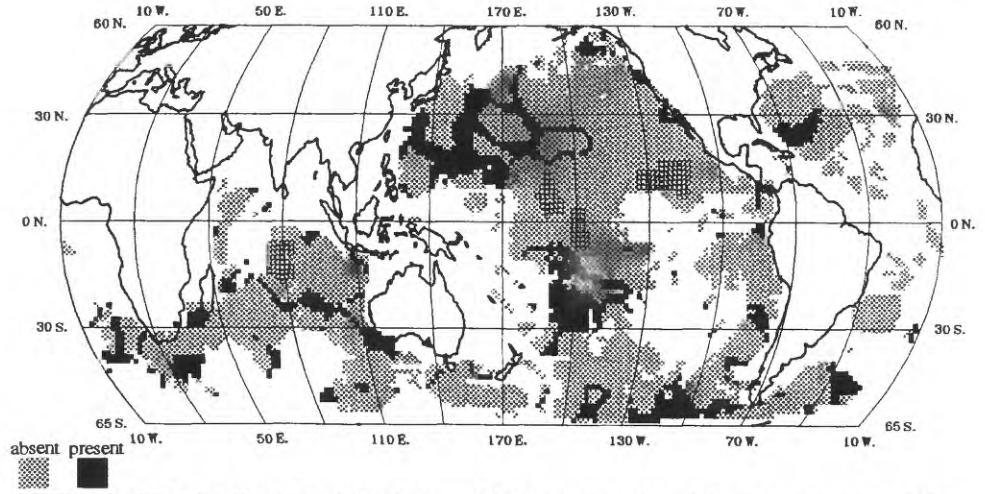

Figure 6d. Distribution of Cu (31st - 50th class numbers) in manganese nodules.

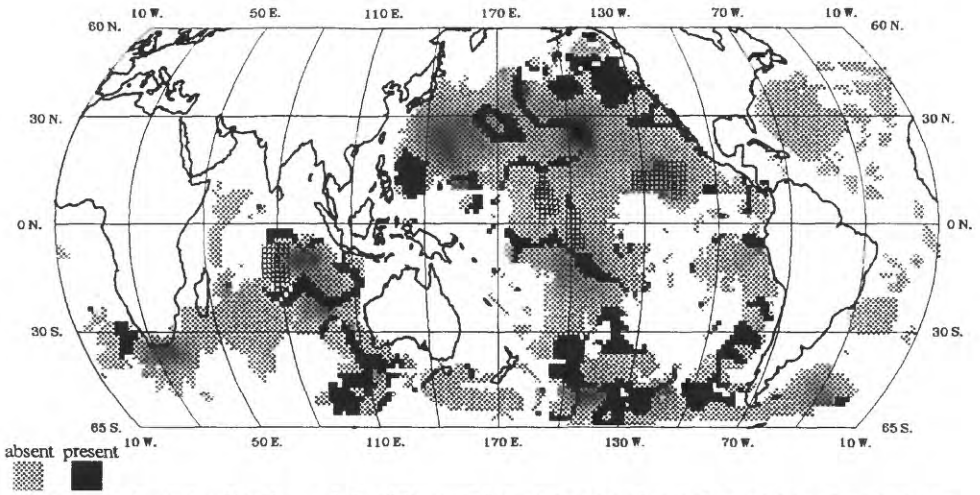

Figure 6e. Distribution of Cu (51st - 70th class numbers) in manganese nodules.

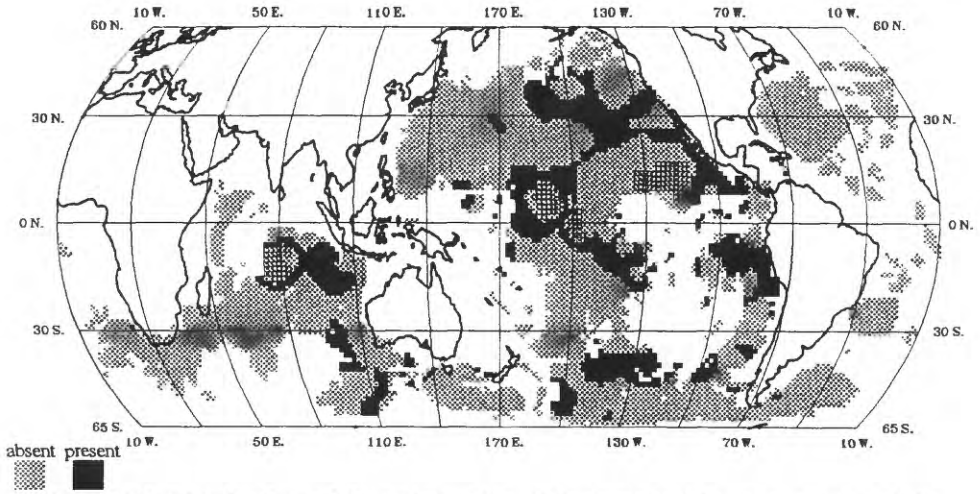

Figure 6f. Distribution of Cu (71st - 90th class numbers) in manganese nodules.

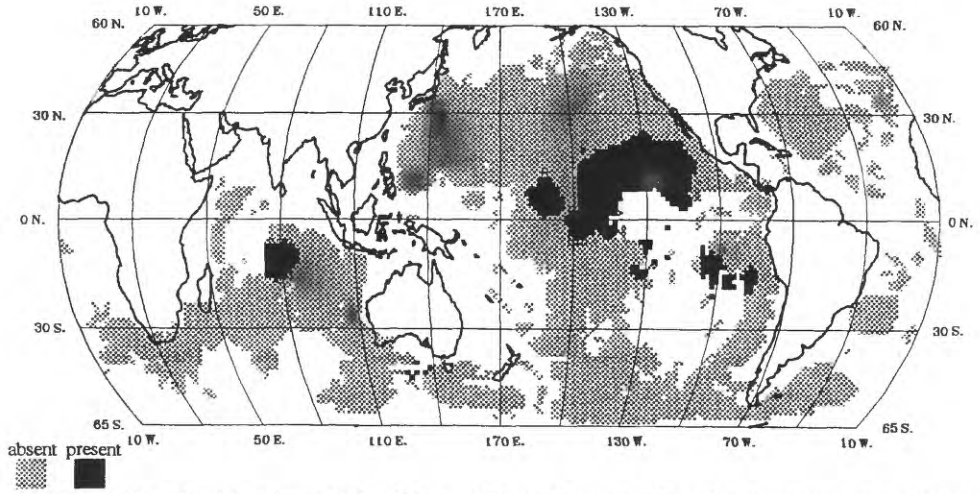

Figure 6g. Distribution of Cu (91st - 100th class numbers) in manganese nodules.

Table 6: Salient features of the disaggregated **Cu** spatial distribution.

Variable	Comments
1^{st} – 10^{th} class numbers	This concentration range is characterized by widely scattered small-medium clusters.
11^{th} – 30^{th} class numbers	A very large irregular cluster trends northeast from the south tip of Africa to southwest of the Indian Ocean model. Two medium clusters occur in northwest Atlantic. A large cluster occurs east of southern tip of South America. A medium cluster intersects southern half of Brazil Basin. Scattered small-medium clusters occur in the north and south Pacific.
31^{st} – 50^{th} class numbers	A large irregular cluster is composed of vestiges of three halos northwest of the Line Islands model, and intersects Northwest Pacific Basin. A large irregular cluster south of the Line Islands model intersects the Penrhyn, Samoan, and Southwest Pacific Basins. An east trending string of small-medium clusters occurs at $\approx$ 60°S., from 170°W. to 70°W. A northwest trending irregular linear extends from southwest Australia to the southwest of the Indian Ocean model.
51^{st} – 70^{th} class numbers	A large irregular thin halo partially encloses the Indian Ocean model. An irregular thin halo, mostly in the Northwest Pacific Basin, is concentric with a larger thin vestigial halo whose southern boundary forms an irregular thin medium halo enclosing the Line Islands model. A northwest trending zone of medium clusters intersects the Chile Basin. Other occurrences are scattered medium-large clusters throughout Pacific and Indian Oceans.
71^{st} – 90^{th} class numbers	Two well-defined contiguous medium and large halos include the Line Islands model and the Clarion-Clipperton model, respectively. A medium cluster surrounds the Indian Ocean model. Remaining occurrences are mostly large clusters in the north central Pacific, Peru basin, and south central Pacific.
91^{st} – 100^{th} class numbers	A large cluster includes the Indian Ocean model. A very large cluster includes the Clarion-Clipperton model and the southern part of the Line Islands model. A medium cluster includes northern part of the Line Islands model.

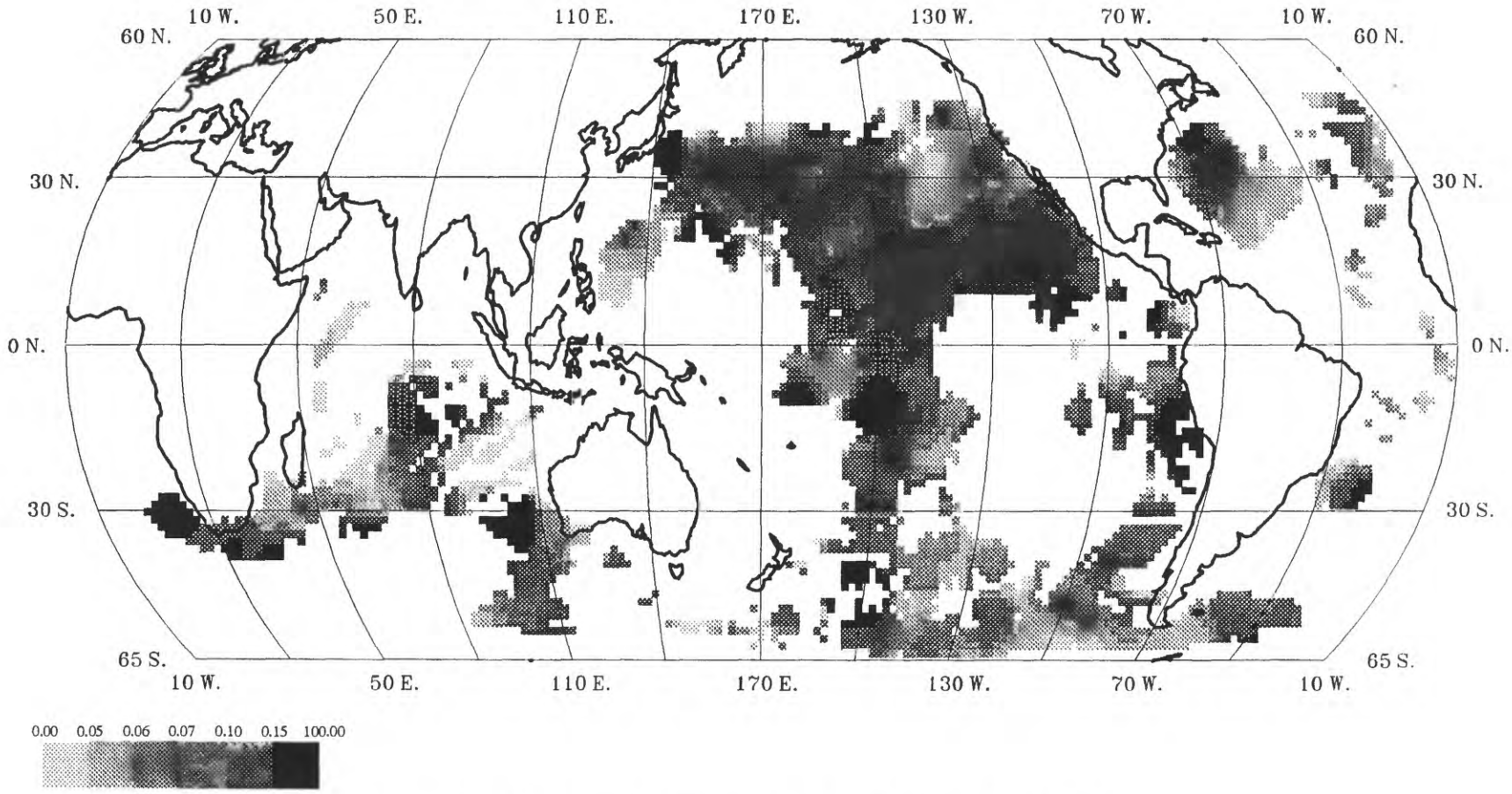

Figure 7a. Distribution of Zn (weight percent) in manganese nodules.

Grey level boundaries represent data values for class numbers 1, 10, 30, 50, 70, 90, and 100.

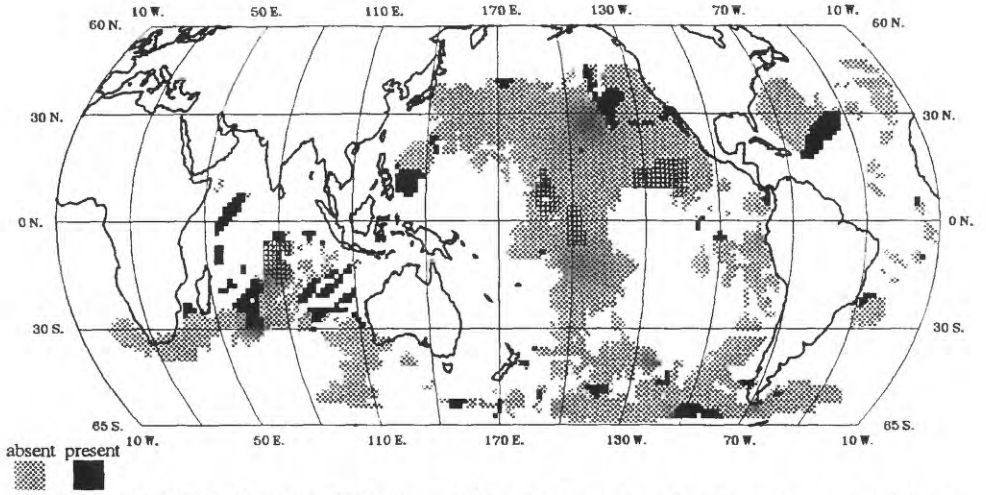

Figure 7b. Distribution of Zn (1st - 10th class numbers) in manganese nodules.

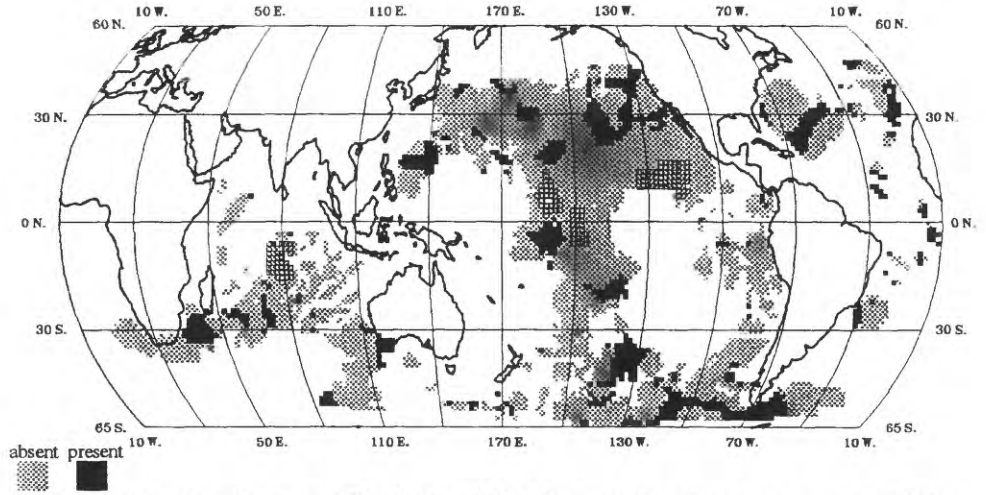

Figure 7c. Distribution of Zn (11th - 30th class numbers) in manganese nodules.

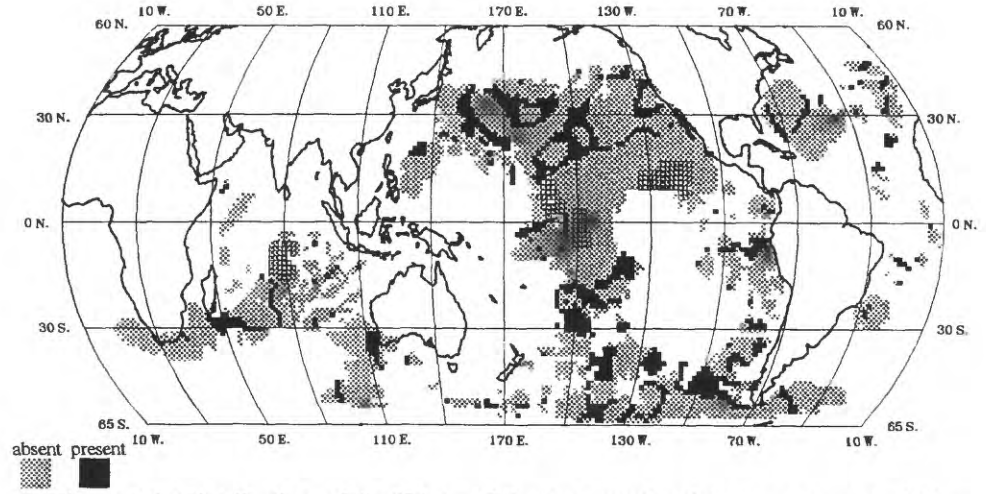

Figure 7d. Distribution of Zn (31st - 50th class numbers) in manganese nodules.

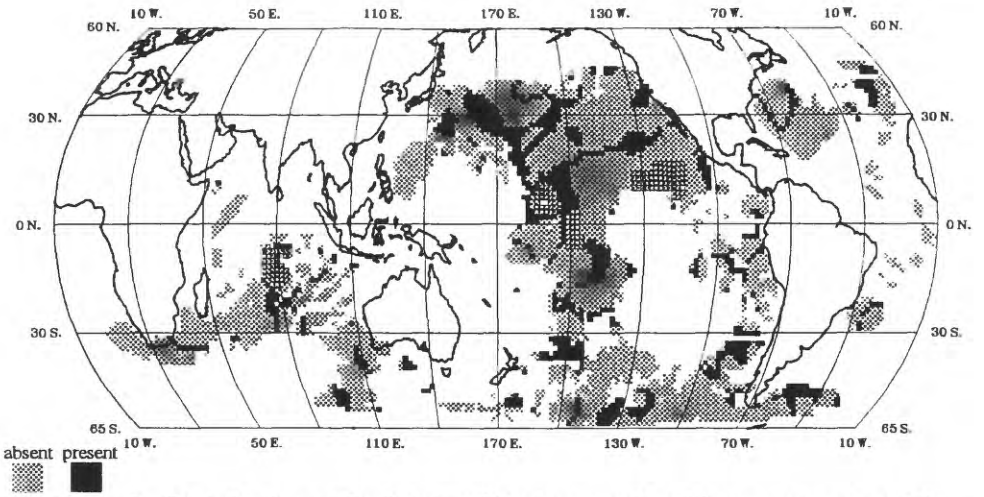

Figure 7e. Distribution of Zn (51st - 70th class numbers) in manganese nodules.

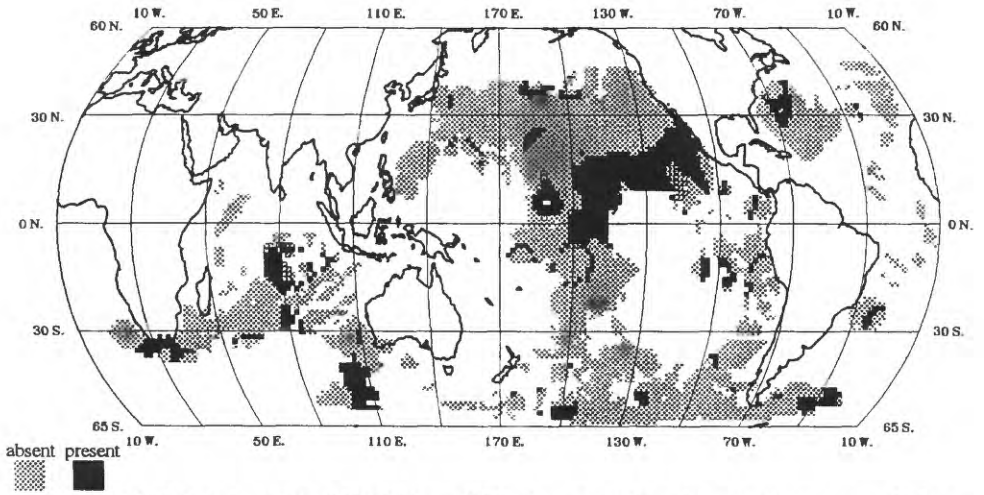

Figure 7f. Distribution of Zn (71st - 90th class numbers) in manganese nodules.

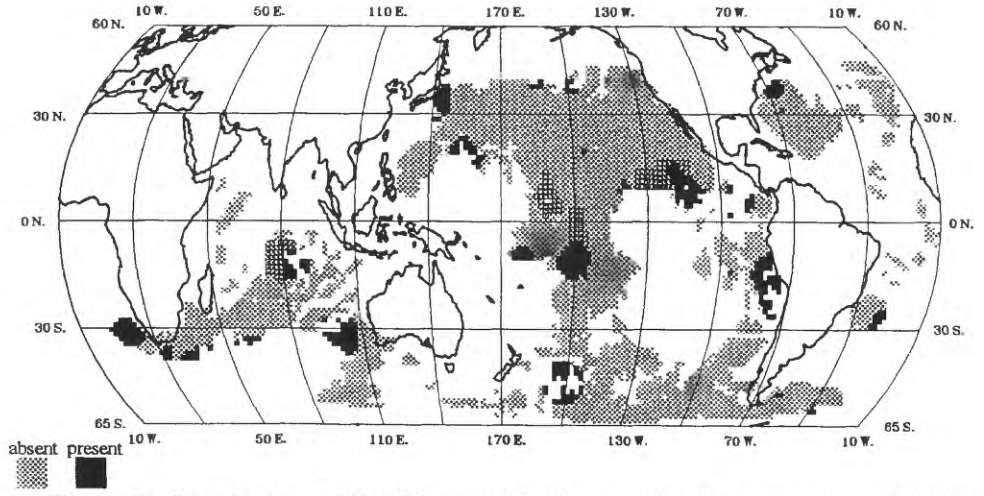

Figure 7g. Distribution of Zn (91st - 100th class numbers) in manganese nodules.

Table 7: Salient features of the disaggregated **Zn** spatial distribution.

Variable	Comments
1^{st} – 10^{th} class numbers	This concentration range is characterized by widely scattered small-medium clusters and linears.
11^{th} – 30^{th} class numbers	This concentration range is characterized by widely scattered small-medium clusters and linears. There is also a northeast trending linear in the Atlantic east of Cuba. An east trending linear occurs at 60°S. from 60° to 130°W. A medium halo occurs west of California at $\approx$ 145°W.
31^{st} – 50^{th} class numbers	Thin irregular linears form vestiges of medium-large halos throughout. The remaining clusters are small and widely scattered.
51^{st} – 70^{th} class numbers	Multiple thin medium-large linear halos occur in north Pacific. A medium halo occurs in the northwest Atlantic. A medium halo encloses the northern and intersects part of the southern Line Islands model. Very small-medium clusters intersect the Indian Ocean model.
71^{st} – 90^{th} class numbers	A very large massive cluster includes most of the Clarion-Clipperton model and the southern part of the Line Islands model. A small cluster includes most of the northern part of the Line Islands model and another includes most of the Indian Ocean model. A small cluster occurs south of Australia and intersects the Southeast Indian Ridge. A small cluster occurs at the southern tip of Africa. A small cluster occurs east of the U.S.
91^{st} – 100^{th} class numbers	Scattered small-medium clusters intersect the Clarion-Clipperton model, the southern Line Islands model, the Peru Basin, east of New Jersey, and the Indian Ocean model. The remaining clusters are mostly very small and widely scattered.

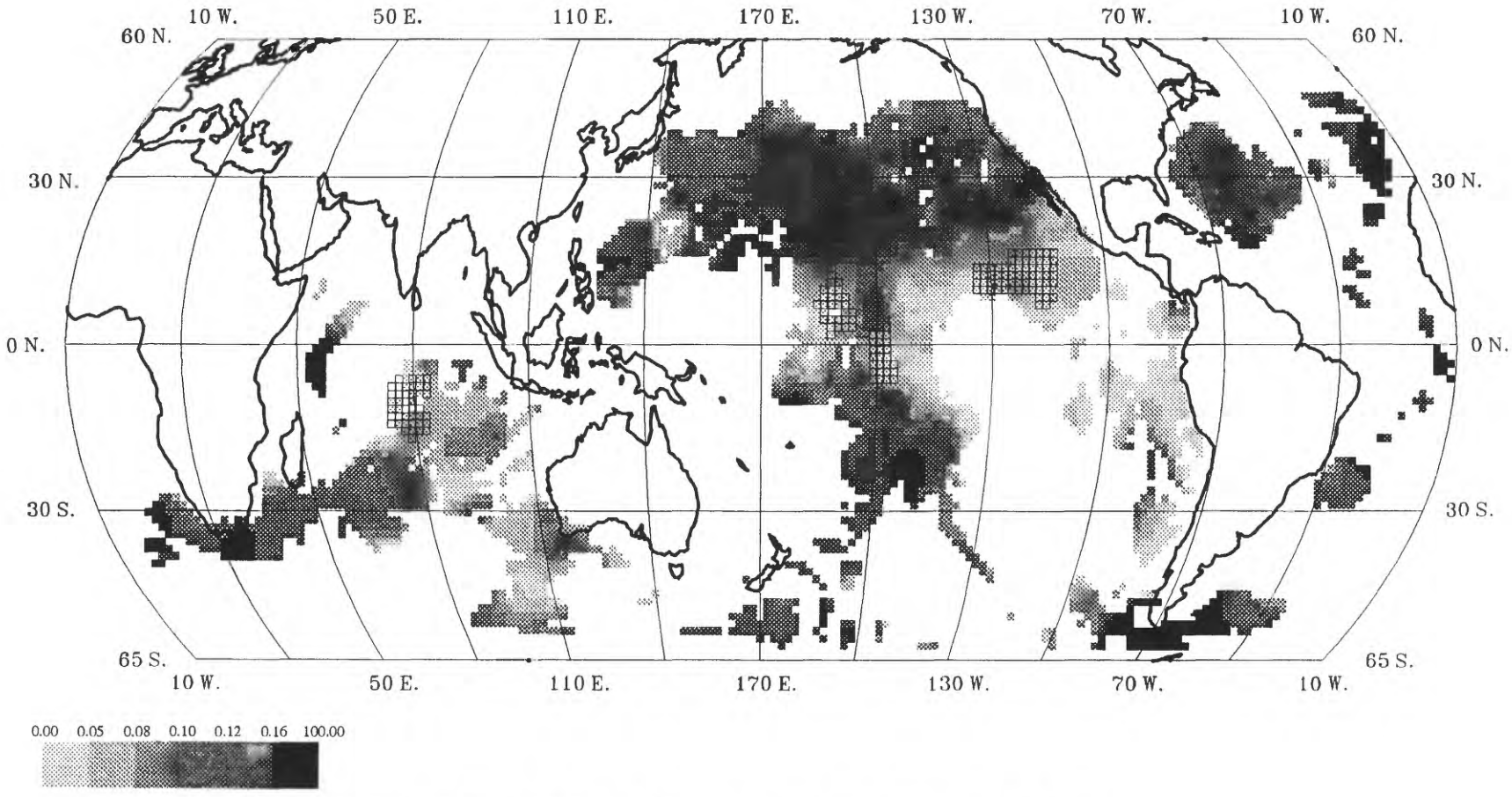

Figure 8a. Distribution of Pb (weight percent) in manganese nodules.

Grey level boundaries represent data values for class numbers 1, 10, 30, 50, 70, 90, and 100.

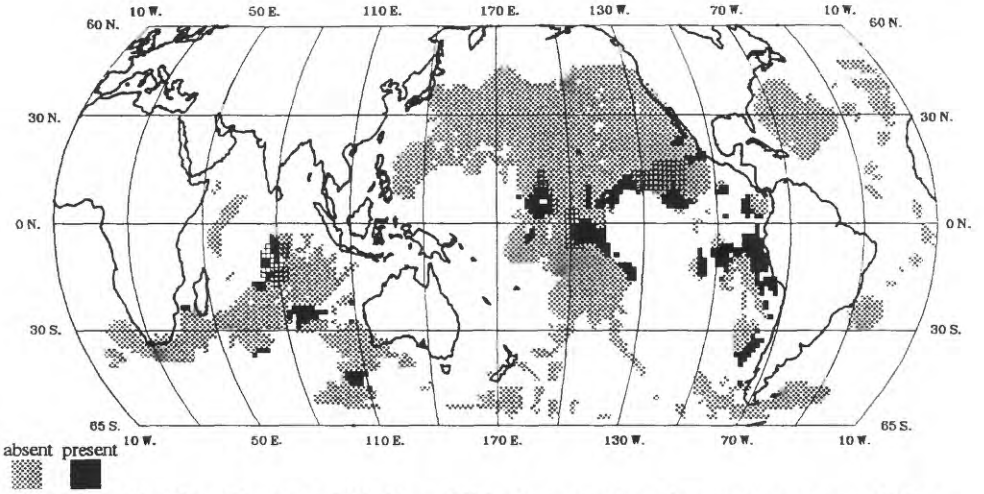

Figure 8b. Distribution of Pb (1st - 10th class numbers) in manganese nodules.

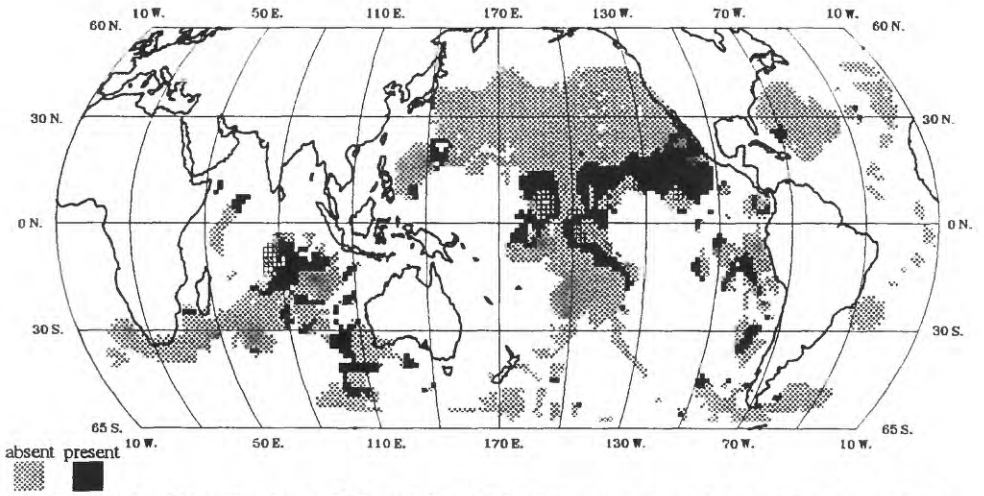

Figure 8c. Distribution of Pb (11th - 30th class numbers) in manganese nodules.

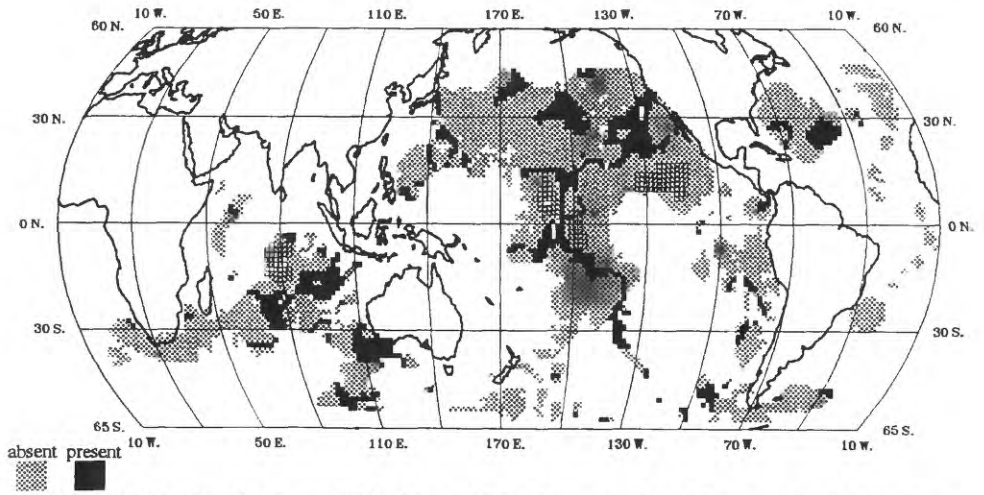

Figure 8d. Distribution of Pb (31st - 50th class numbers) in manganese nodules.

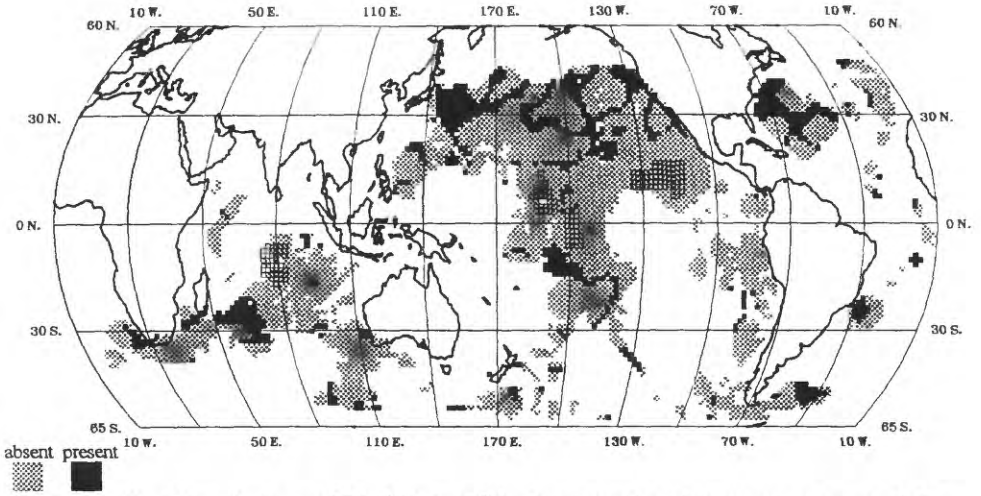

Figure 8e. Distribution of Pb (51st - 70th class numbers) in manganese nodules.

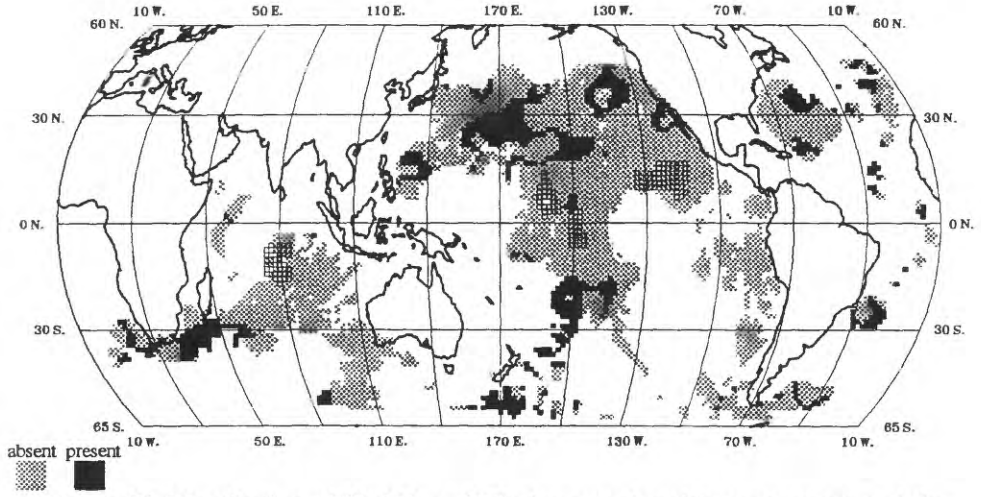

Figure 8f. Distribution of Pb (71st - 90th class numbers) in manganese nodules.

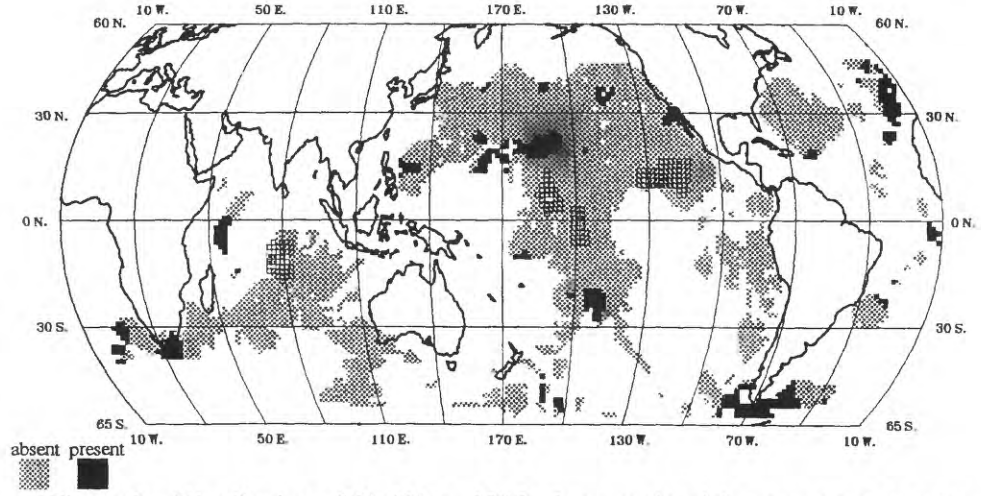

Figure 8g. Distribution of Pb (91st - 100th class numbers) in manganese nodules.

Table 8: Salient features of the disaggregated **Pb** spatial distribution.

Variable	Comments
1^{st} – 10^{th} class numbers	This concentration range is composed of mostly scattered small-medium clusters, many of which intersect the Line Islands model, the Indian Ocean model, and the Clarion-Clipperton model. Others intersect the Chile Basin, and the Peru Basin.
11^{th} – 30^{th} class numbers	A large east trending cluster intersects most of the Clarion-Clipperton and southern Line Islands models. A northwest trending linear intersects the southern Line Islands model. A small halo occurs around the northern Line Islands model. A small cluster intersects the eastern part of the Indian Ocean model. The remaining clusters are widely scattered and very small .
31^{st} – 50^{th} class numbers	Three medium-large clusters trend northwest across the northern Pacific. Thin, irregular vestigial halos occur around the northern Line Islands model area. A large, irregular, thin arcuate linear encloses the southern Line Islands and the western Clarion-Clipperton models. Two medium clusters trend northeast south of the Indian Ocean model. A medium cluster intersects the Perth and South Australian Basins, and the Diamantina Fracture Zone. A medium cluster occurs east of Cuba. The remaining clusters are widely scattered and small.
51^{st} – 70^{th} class numbers	An east trending zone of medium-large clusters and halos occurs across the northern Pacific. An irregular arcuate medium linear occurs south of the Line Islands model. A medium-large cluster occurs in the western north Atlantic. A medium cluster intersects the Madagascar Basin. The remaining clusters are widely scattered and small .
71^{st} – 90^{th} class numbers	Medium-large clusters occur in east trending zones across the northern Pacific and south of Madagascar. A north trending zone of medium clusters occurs in the south central Pacific. The remaining clusters are widely scattered and small .
91^{st} – 100^{th} class numbers	Medium clusters occur south of Argentina, north of the Line Islands model, and south of Africa. The remaining clusters are small-medium and widely scattered.

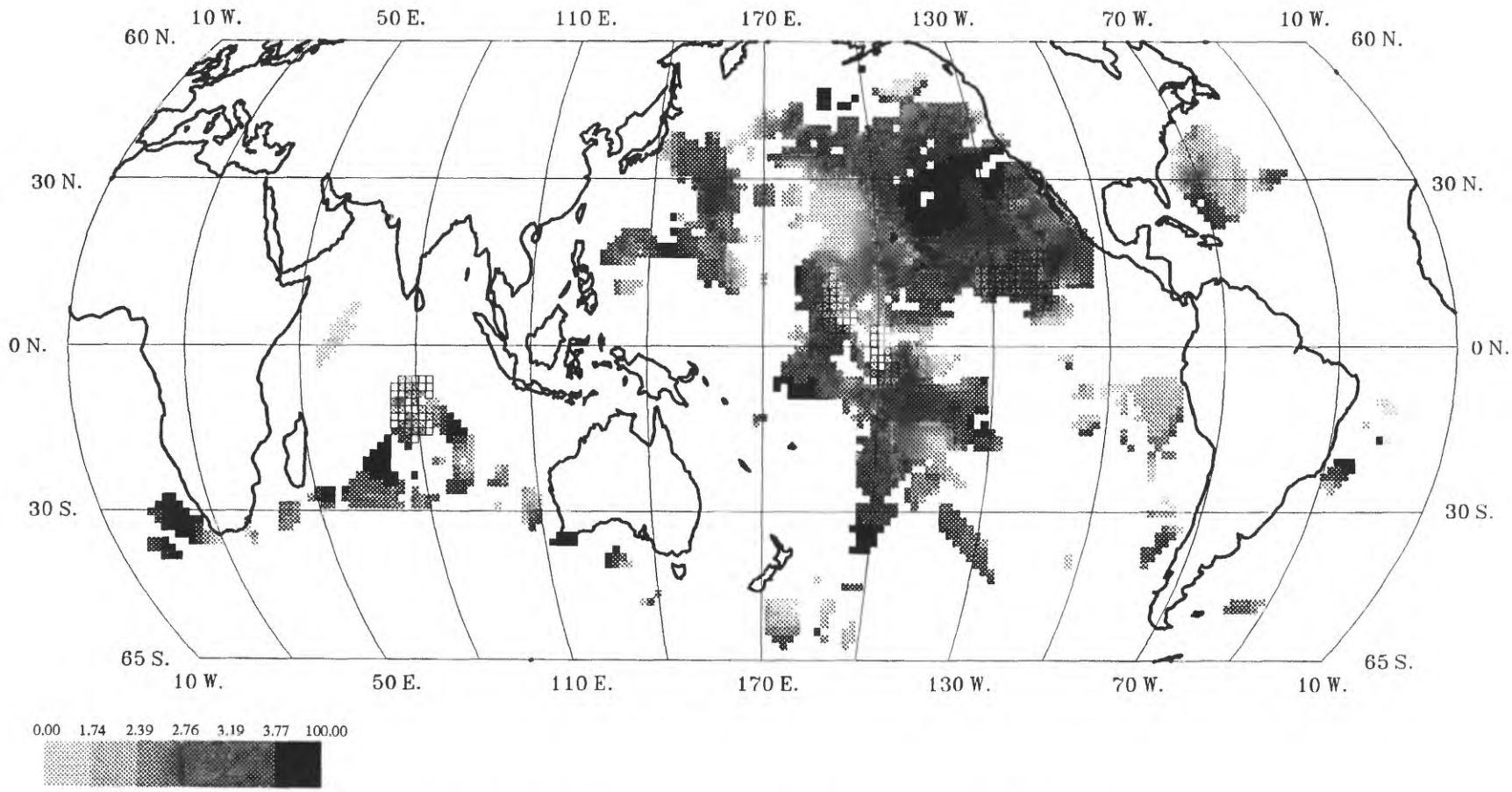

Figure 9a. Distribution of Al (weight percent) in manganese nodules.

Grey level boundaries represent data values for class numbers 1, 10, 30, 50, 70, 90, and 100.

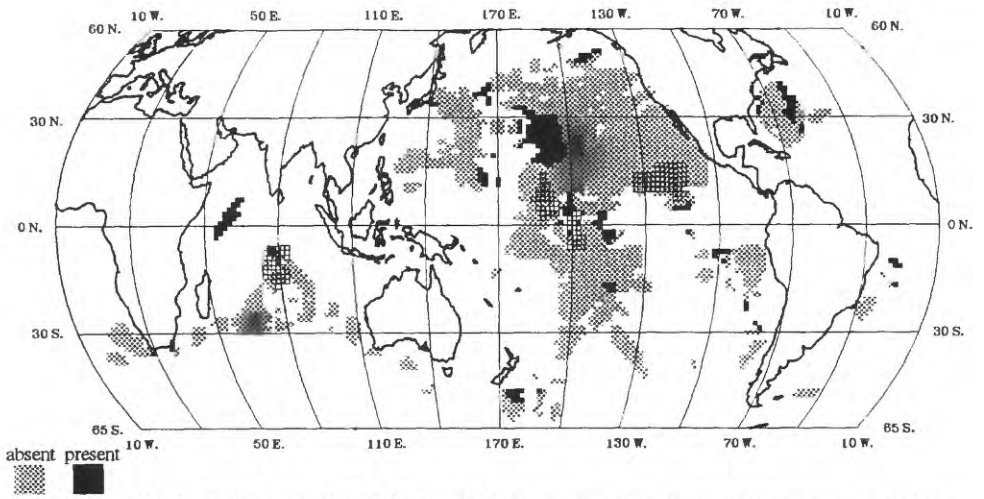

Figure 9b. Distribution of Al (1st - 10th class numbers) in manganese nodules.

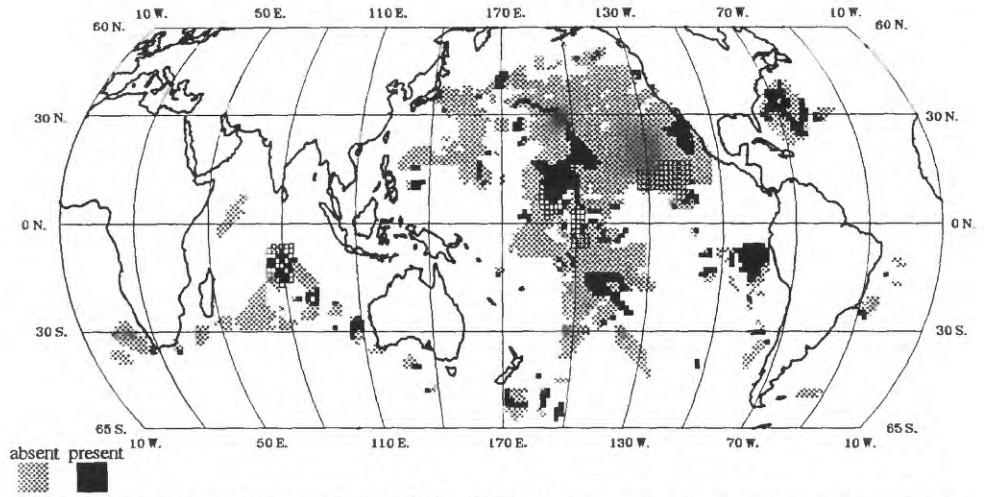

Figure 9c. Distribution of Al (11th - 30th class numbers) in manganese nodules.

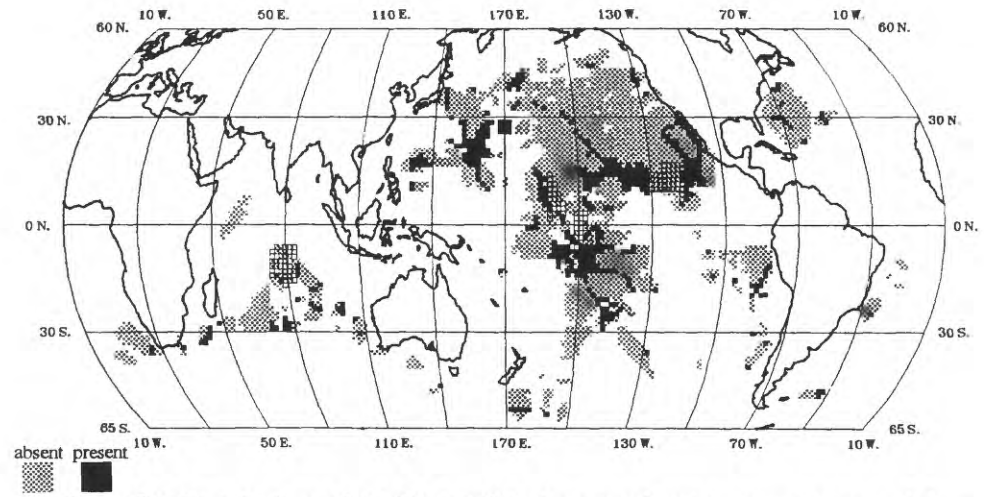

Figure 9d. Distribution of Al (31st - 50th class numbers) in manganese nodules.

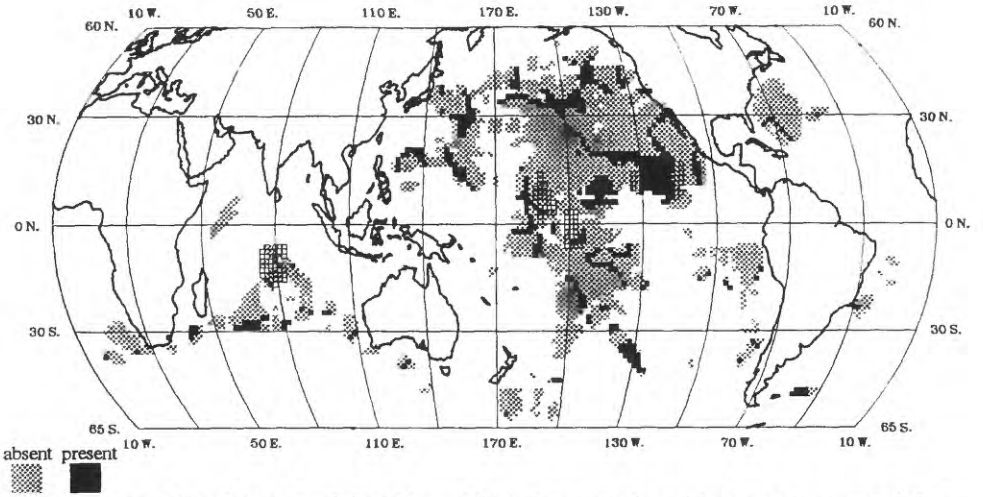

Figure 9e. Distribution of Al (51st - 70th class numbers) in manganese nodules.

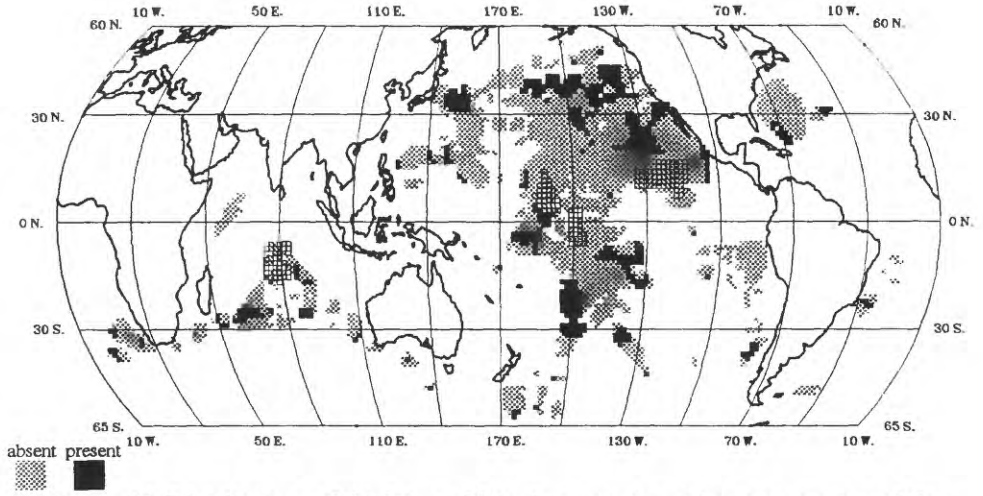

Figure 9f. Distribution of Al (71st - 90th class numbers) in manganese nodules.

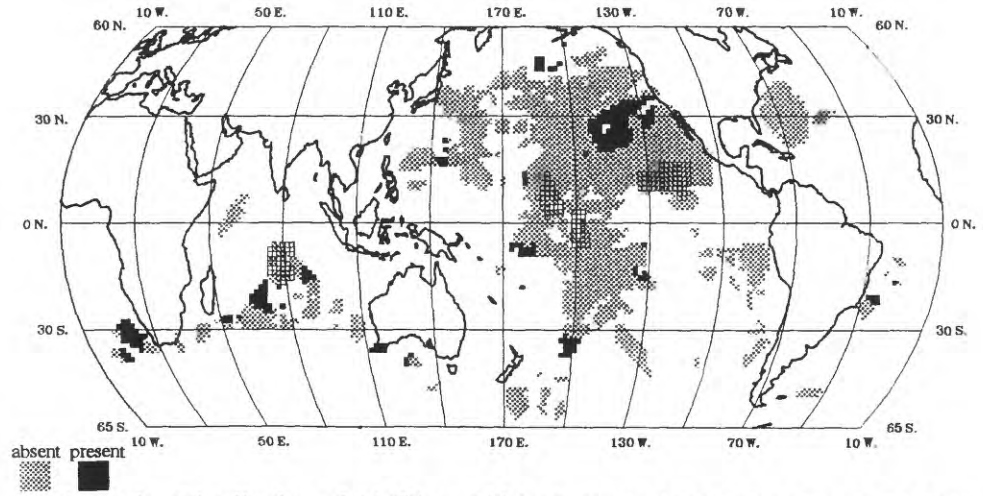

Figure 9g. Distribution of Al (91st - 100th class numbers) in manganese nodules.

Table 9: Salient features of the disaggregated **Al** spatial distribution.

Variable	Comments
1^{st} – 10^{th} class numbers	This concentration range is characterized by few widely scattered small clusters and a medium cluster north of the Line Islands model.
11^{th} – 30^{th} class numbers	A small cluster occurs in the Indian Ocean model. A medium cluster intersects the northern Line Islands model. Other clusters are small-medium and are widely scattered.
31^{st} – 50^{th} class numbers	A medium cluster occurs in the Northwest Pacific Basin. Three northwest trending small-medium linears intersect the Line Islands model, and the eastern end and western end of the Clarion-Clipperton model. The remaining clusters are small and widely scattered.
51^{st} – 70^{th} class numbers	A large cluster is included in the Clarion-Clipperton model. Small northwest trending thin linears occur in Pacific and northern Atlantic. Small-medium clusters occur across the northern Pacific.
71^{st} – 90^{th} class numbers	Medium clusters occur in a southeast trending zone across the northern Pacific. A small cluster intersects the Line Islands model. The remaining clusters are small and widely scattered.
91^{st} – 100^{th} class numbers	A large cluster occurs northwest of the Clarion-Clipperton model. The remaining few clusters are small and widely scattered.

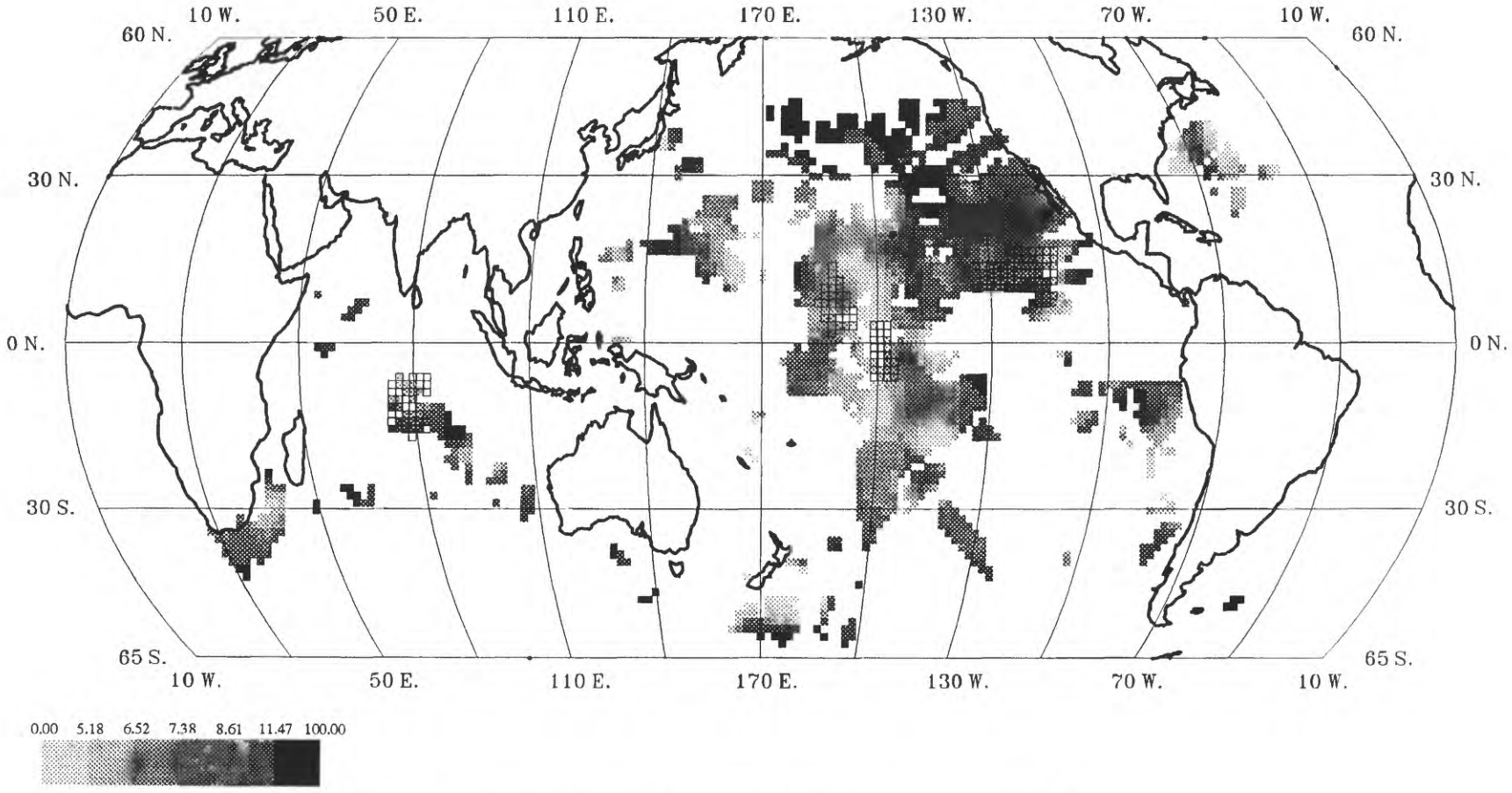

Figure 10a. Distribution of Si (weight percent) in manganese nodules.

Grey level boundaries represent data values for class numbers 1, 10, 30, 50, 70, 90, and 100.

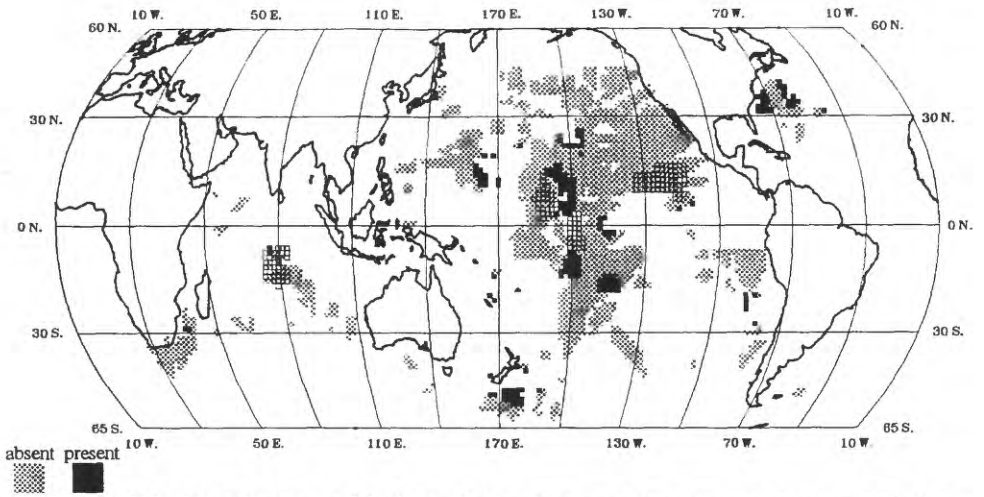

Figure 10b. Distribution of Si (1st - 10th class numbers) in manganese nodules.

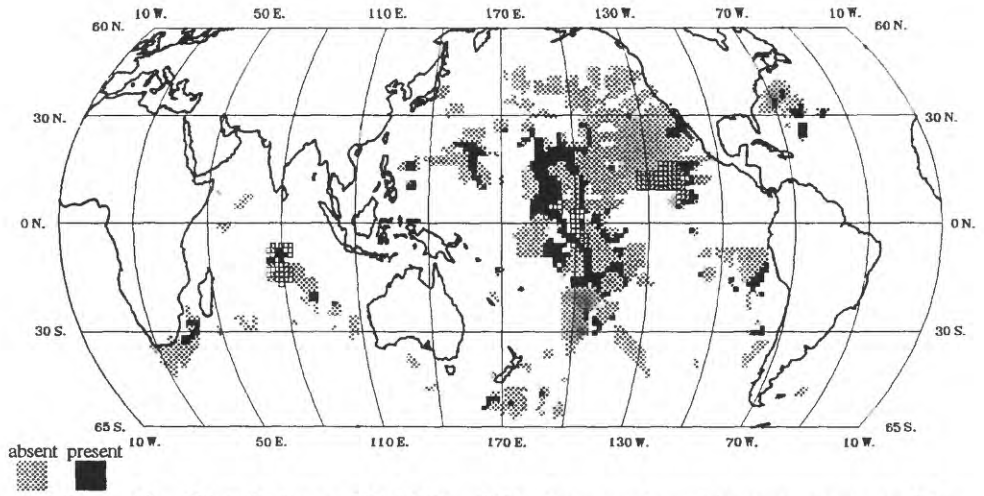

Figure 10c. Distribution of Si (11th - 30th class numbers) in manganese nodules.

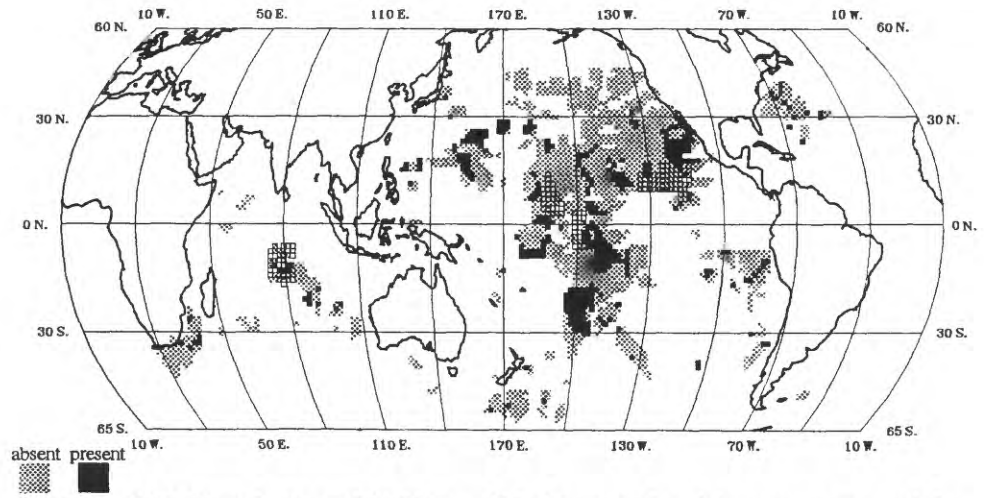

Figure 10d. Distribution of Si (31st - 50th class numbers) in manganese nodules.

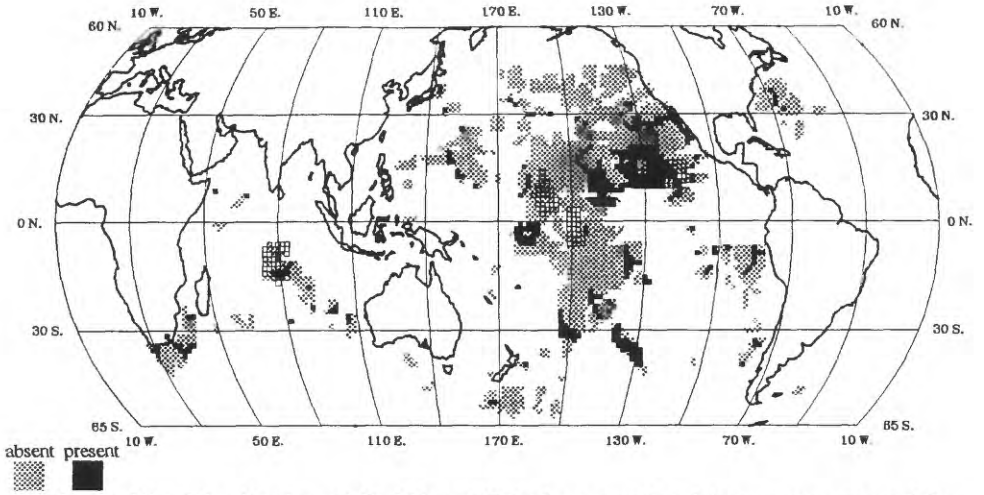

Figure 10e. Distribution of Si (51st - 70th class numbers) in manganese nodules.

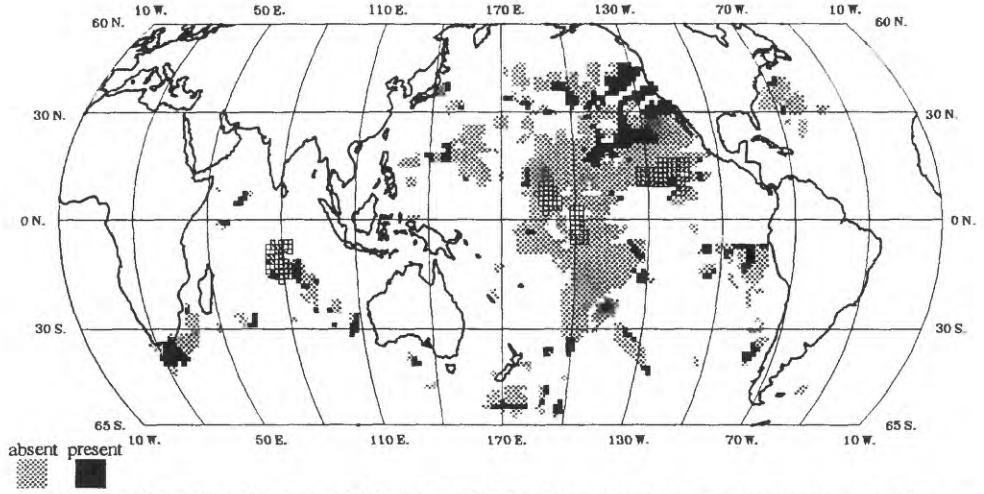

Figure 10f. Distribution of Si (71st - 90th class numbers) in manganese nodules.

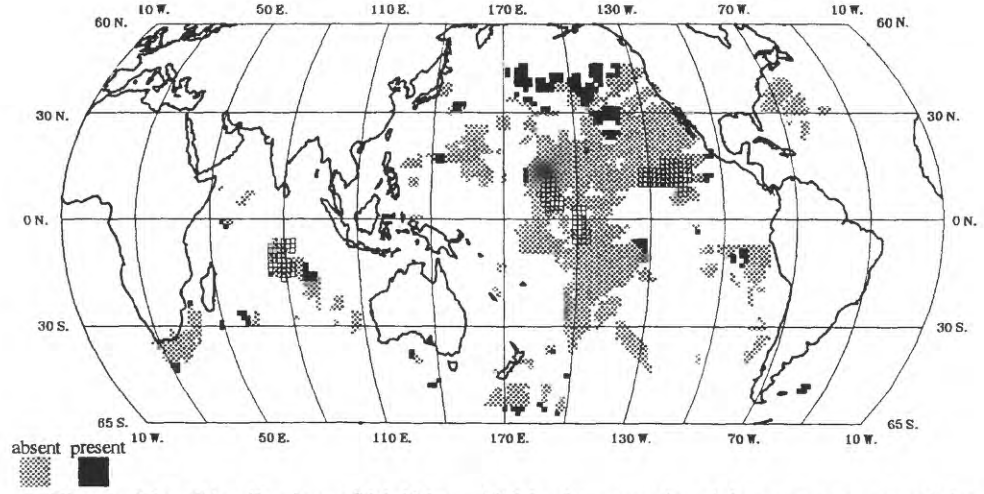

Figure 10g. Distribution of Si (91st - 100th class numbers) in manganese nodules.

Table 10: Salient features of the disaggregated **Si** spatial distribution.

Variable	Comments
1^{st} – 10^{th} class numbers	A north trending zone of small clusters intersects the Line Islands model. The remaining clusters are few and widely scattered.
11^{th} – 30^{th} class numbers	A very small cluster occurs within the Indian Ocean model. A medium northwest trending linear halo intersects most of the northern and part of the southern Line Islands model. A small cluster intersects the eastern Clarion-Clipperton model.
31^{st} – 50^{th} class numbers	Small-medium clusters intersect the Line Islands model and the northern Clarion-Clipperton model. Remaining clusters are mostly small and widely scattered.
51^{st} – 70^{th} class numbers	A large cluster includes most of the western Clarion-Clipperton model. Remaining clusters are small and widely scattered.
71^{st} – 90^{th} class numbers	Irregular patchwork of small-medium clusters occur in the northeastern Pacific. Remaining clusters are very small and widely scattered.
91^{st} – 100^{th} class numbers	East trending patchwork of small-medium clusters occur in north Pacific. Remaining clusters are very small and very widely scattered.

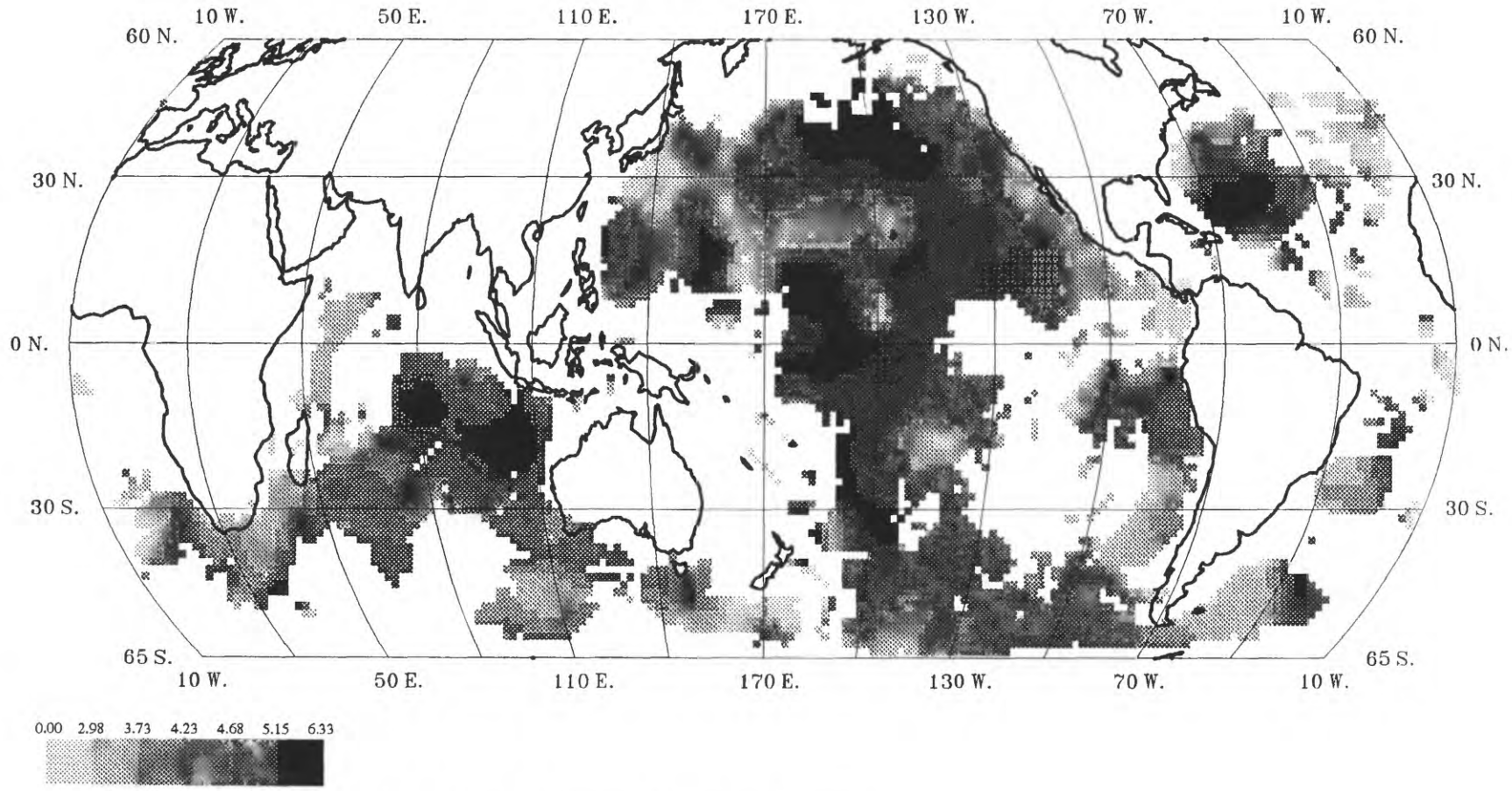

Figure 11a. Distribution of sample depth (meters).

Grey level boundaries represent data values for class numbers 1, 10, 30, 50, 70, 90, and 100.

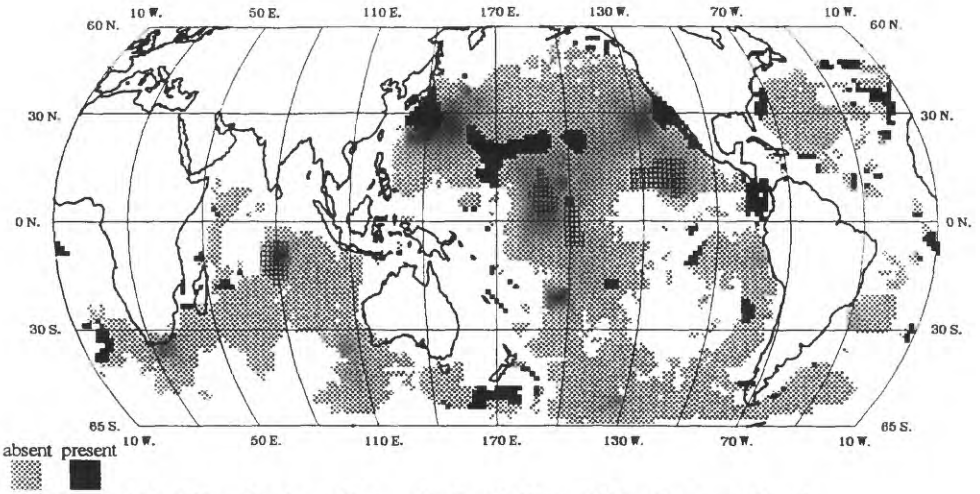

Figure 11b. Distribution of sample depth (1st - 10th class numbers).

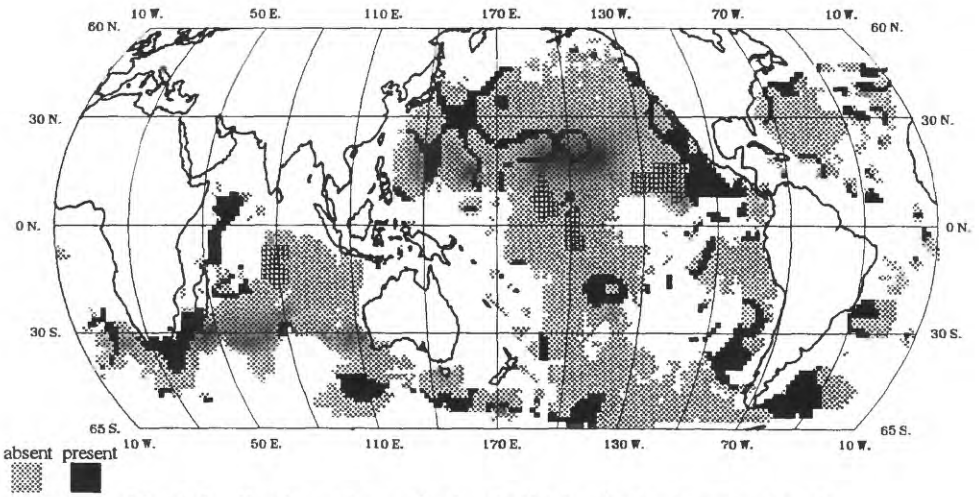

Figure 11c. Distribution of sample depth (11th - 30th class numbers).

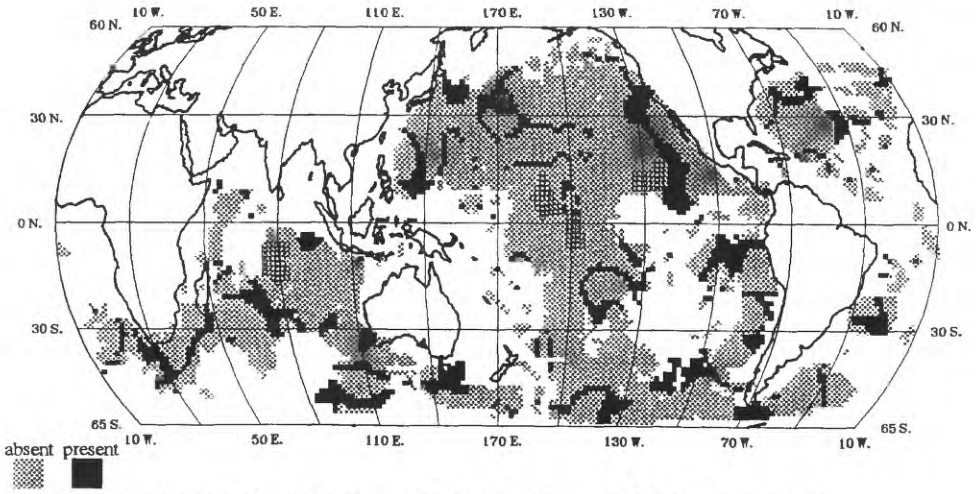

Figure 11d. Distribution of sample depth (31st - 50th class numbers).

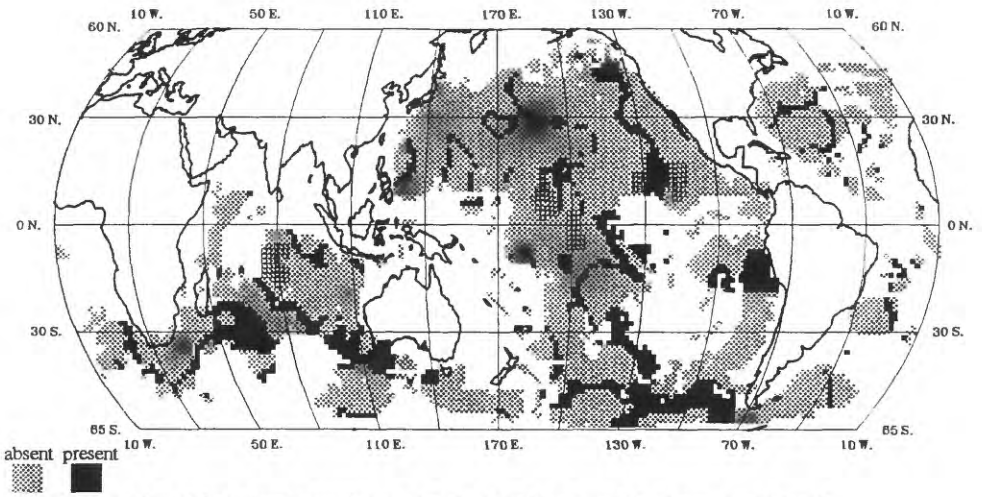

Figure 11e. Distribution of sample depth (51st - 70th class numbers).

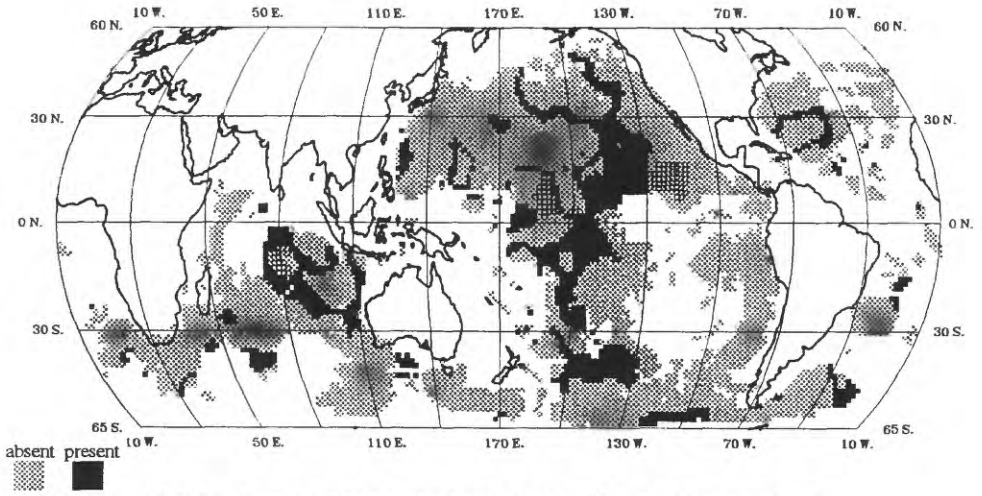

Figure 11f. Distribution of sample depth (71st - 90th class numbers).

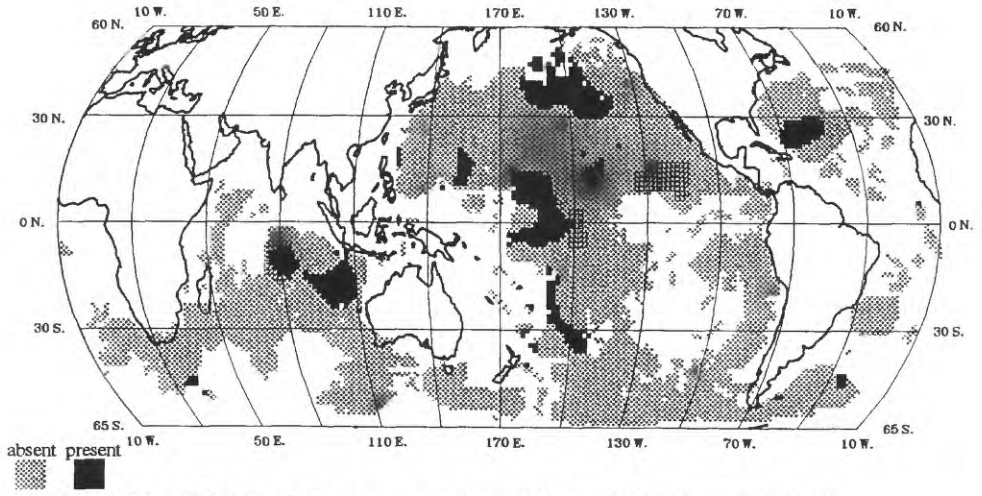

Figure 11g. Distribution of sample depth (91st - 100th class numbers).

Table 11: Salient features of the disaggregated **sample depth** spatial distribution.

Variable	Comments
1^{st} – 10^{th} class numbers	Four medium-large clusters occur across the northern Pacific. A medium cluster is adjacent to central America. Remaining clusters are small and widely scattered.
11^{th} – 30^{th} class numbers	A semi-continuous medium arcuate linear occurs around the south tip of Africa. A medium cluster intersects Chile Basin. A large cluster occurs east of southern Argentina. A large cluster intersects the east end of the Clarion-Clipperton model. Medium linear clusters occur across the northwest Pacific. Remaining clusters are small-medium and widely scattered.
31^{st} – 50^{th} class numbers	A large northwest trending linear intersects the eastern Clarion-Clipperton model. Small-medium irregular linears and halos occur throughout.
51^{st} – 70^{th} class numbers	A northwest trending large linear intersects the Clarion-Clipperton model. A medium northwest trending linear is almost completely coincident with the SE. Indian Ridge. A large cluster occurs southeast of Madagascar. A large east trending irregular linear occurs across the southeastern Pacific. A large thin linear halo occurs in the western Atlantic. Remaining clusters are small and widely scattered.
71^{st} – 90^{th} class numbers	A very large north trending zone from ≈50°S. to ≈50°N. encloses the southern Line Islands model and intersects the northern Line Islands and western Clarion-Clipperton models. A medium halo occurs around the Indian Ocean model. A medium linear halo occurs east of Florida (cf. 50th to 70th class numbers).
91^{st} – 100^{th} class numbers	A medium cluster occurs in and another one occurs east of the Indian Ocean model. A large cluster includes the northern and part of the southern Line Islands model. A large cluster occurs in the northern central Pacific. A medium cluster occurs east of Florida. A north trending medium linear occurs south of the Line Islands model. The very few remaining clusters are small and widely scattered.

Selected case studies

The following examples show some advantages of using both the composite and disaggregated maps to describe the spatial distributions of cobalt and nickel, two nodule components considered to be of major economic importance. This example is based on maps of their spatial distributions as compared with those of depth.

Cobalt

It is obvious from the composite and disaggregated maps (fig. 2) that the areas of highest cobalt content ($\geq 91^{st}$ class number, fig. 2g) are coincidental with areas of sample depths ranging from the first (i.e., most shallow) through the 50^{th} class number (fig. 11b-11d) However, this range of low depths also occurs in areas where there is no appreciable cobalt. These relations are evident in the composite maps but not as distinctly as they are on the disaggregated ones. This is particularly true on the moderate to high cobalt concentrations (71^{st} to 100^{th} class numbers).

Thus, in the case of cobalt as related to depth, in selecting target areas or inspecting the components for a multivariate analysis, one is more likely to commit a pre-quantitative analysis of erroneously selecting a barren area by not using the disaggregated maps.

Nickel

The relationship between nickel (fig. 3) and sample depth (fig. 11) is not as straightforward as that of cobalt. The 31^{st} to 90^{th} class numbers of sample depth contain the 71^{st} to 100^{th} class numbers of nickel. The areas of depth class numbers, without correlative high nickel, occur over broad areas across the entire study region. Therefore, if depth is to be used with nickel as a simple two-component guide for data capture, the analysis would be greatly enhanced by use of both types of maps. In this way, each disaggregated segment can be easily compared with each other segment as well as with the complete picture presented in the composite. The major objective would be to cast out those areas that indicate no potential for nickel. and retain the higher nickel potential areas for later study.

Conclusions

Most of the areas of data extremes are well portrayed in both the composite and the disaggregated maps. However, particularly at the intermediate concentration ranges and very small scales used here, there is a reasonable chance that some significant target areas may be overlooked by using the composite maps alone. Disaggregated maps are very well suited to the resolution of this problem. Also, use of color instead of grey-levels for composite maps would help to solve this problem on appropriately equipped computers.

Multivariate analytical methods involve variables for the full range of their values. As is shown in the previous examples, disaggregated maps portray the full range of data values, particularly in the middle data ranges, more clearly

and distinctly than composite maps. In this regard, the analyst has more opportunity to observe more data relationships between variables than by using composite maps alone.

Beacuse each grid square on the maps presented here is approximately 125 miles on each side, it is obvious that marine resource data capture is very costly, and planners of field work must make every effort to minimize the likelihood capture of data from areas that are apparently viable with respect to presence of mineral resources, but are truly barren in this regard.

References

Botbol, J.M., 1990, A Cu-Zn-Mn-Zn mineral resource model for the northern Pacific Oceanic Basin: U.S. Geological Survey Open File Report 90-402, 25p.

Botbol, J.M. and Evenden, G.I., 1989, Descriptive statistics and spatial distributions of geochemical variables associated with manganese oxide-rich phases in the northern Pacific: U.S. Geological Survey Bulletin 1863, 62p.

Evenden, G.I., 1990, Cartographic projection procedures for the UNIX environment—A user's manual: U.S. Geological Survey Open File Report OF90-284, 63p.

Frazer, J.Z., and Fisk, M.B., 1980, Availability of copper, nickel, cobalt, and manganese from ocean ferromanganese nodules (III): La Jolla, Calif., Scripps Institution of Oceanography, SIO reference 80-16 (prepared for U.S. Bureau of Mines), 117p.

Lenoble, J., 1992, Future deep-sea bed mining of polymetallic nodules ore deposits: XV world Mining Congress, Madrid, Spain, 9p.

McKelvey, V.E., Wright, N.A., Bowen, R.W., 1983, Analysis of the world distribution of metal-rich subsea manganese nodules: U.S. Geological Survey Circular 886, 55p.